Supporting Information for

Direct Resonance Raman Characterization of a Peroxynitrito Copper Complex Generated from O_2 and NO and Mechanistic Insights into Metal Mediated Peroxynitrite Decomposition

Jeffrey J. Liu,[a] Maxime A. Siegler,[a] Kenneth D. Karlin,*[a] and Pierre Moënne-Loccoz*[b]

[a]*Department of Chemistry, Johns Hopkins University, Baltimore, Maryland 21218, United States*

[b]*Department of Biochemistry & Molecular Biology, Oregon Health & Science University, Portland, Oregon 97239, United States*

Contents

1 Experimental

1.1 General Methods

All reagents and solvents used were purchased from commercial sources unless stated otherwise. Inhibitor free 2-methyltetrahydrofuran (MeTHF) was purchased from Sigma-Aldrich and distilled under an argon atmosphere from sodium benzophenone. All synthetic manipulations were performed in a N_2 filled glovebox (Vacuum Atmospheres, O_2 < 0.3 ppm). Glassware was dried for at least 30 minutes in a 120 ºC oven before use. $^{16}O_2$ was purchased from Airgas (Ultra High Purity) and used after passing through a Drierite column. $^{14}N^{16}O$ was purchased from Matheson Gases and purified following methods previously described.[1] Purified NO was stored in a 50 mL Schlenk flask capped with a rubber septum. $^{18}O_2$ (98 atom % ^{18}O) and $^{15}N^{18}O$ (98.1 atom % ^{15}N, 99.7 atom % ^{18}O) were both purchased from ICON Isotopes (Dexter, MI). A lecture bottle of nitrogen dioxide was purchased from Sigma-Aldrich and used without further purification. Deoxygenation of solvents for glovebox use were performed by bubbling the solvent in an addition funnel with $Ar_{(g)}$ for 30-45 min and transferred to the glovebox in a Strauss flask. MeTHF was stored in the glovebox under 4Å molecular sieves. $[Cu^{I}(TMG_3tren)]B(C_6F_5)_4$ and $F_8Fe^{II}(H_2O)$ [F_8 = tetrakis(2,6-difluoro-phenyl)porphyrinate(2–)] were prepared according to literature methods.[2,3] Nitrite was detected using a Molecular Probes Griess Reagent Kit (ThermoFisher G7921). Elemental analyses were performed either by Micro-Analysis Inc. (Wilmington, DE) or Midwest Microlabs (Indianapolis, IN).

Instrumentation

All UV-vis experiments were performed on a Cary-50 Bio spectrophotometer equipped with a Unisoku USP-203A cryostat using a modified 1 cm pathlength Schlenk cuvette. EPR spectra were collected with an ER 073 magnet equipped with a Bruker ER041 X-Band microwave bridge and a Bruker EMX 081 power supply: microwave frequency = 9.42 GHz, microwave power = 0.201 mW, attenuation = 30 db, modulation amplitude = 10 G, modulation frequency = 100 kHz, temperature = 20 K. Gas chromatography (GC) was performed on an Agilent 6890N gas chromatograph using a DB-5 5% phenylmethyl siloxane capillary column and equipped with a flame-ionization detector (FID). Electrospray Ionization Mass Spectrometry (ESI-MS) was performed on a Thermo Finnigan LCQ Deca XP-Plus (Thermo Finnigan, San Jose, CA) with capillary heated to 250 ºC and the spray voltage set to 4.5 kV. Single-crystal X-ray data were collected using either an Xcalibur3 or a SuperNova (Agilent Technologies) diffractometer at the Johns Hopkins University X-ray diffraction facility.

Preparation of Samples for Resonance Raman Spectroscopy and Data Collection

In the glovebox $[Cu^{I}(TMG_3tren)]B(C_6F_5)_4$ (48.6 mg, 0.041 mmol) was dissolved in 5 mL of MeTHF (8.2 mM). Aliquots of this solution (0.3 mL) were added to NMR tubes (5 mm O.D.) and sealed with rubber septa and parafilm. The samples oxygenated at –130 ºC and excess O_2 removed via sparging with $Ar_{(g)}$. $NO_{(g)}$ (5 mL) was then injected into the sample using a 3-way gas tight syringe and the solution was allowed to react for 30 min before freezing in liquid nitrogen. The isotopically labeled samples were prepared using the same methods where $^{18}O_2$ and $^{15}N^{18}O$ were substituted for $^{16}O_2$ and $^{14}N^{16}O$.

Resonance Raman spectra were obtained on a custom McPherson 2061/207 spectrometer equipped with a Princeton Instrument liquid-N_2-cooled CCD detector (LN-1100 PB). A Semrock

RazorEdge filter was used to attenuate Rayleigh scattering. The excitation source consisted of a krypton ion laser 407-nm line. The laser intensity was set at or below 10 mW and was loosely focused with a cylindrical lens to illuminate an area of 10 mm by 0.2 mm at the bottom of the sample in the NMR tube. The NMR tube was maintained at ~110 K inside a copper coldfinger cooled with liquid nitrogen and was spun continuous to minimize photochemistry and bleaching of chromophoric complexes. Frequencies were calibrated relative to aspirin and are accurate to ± 1 cm^{-1}.

Computational Methods

All density functional theory calculations were performed using the Gaussian 09, version D.01 software package. All calculations were performed using the b3lyp functional under the spin-unrestricted formalism and using the def2-TZVP basis set for all atoms. Where available, X-ray crystal structures were used as initial starting geometry guesses. Analytical frequency calculations using identical level of theory and basis set confirmed the converged structures were true minima (i.e. no imaginary frequencies were observed). Analytical Raman calculations were carried out using the command "freq=Raman" in Gaussian 09 and processed using Gaussview 5.0.9. EPR fitting was performed using EasySpin version 5.2.23 in MatLab (R2017a).

Handling and Transfer of $^{18}O_2$, $^{15}N^{18}O$, and NO_2

Labeled dioxygen, nitric oxide and unlabeled nitrogen dioxide were supplied as gasses in lecture bottles and transferred to 50 mL Schlenk flasks sealed with rubber septa and used without further purification. In a typical transfer, a Schlenk flask was connected to the lecture bottle regulator through a short length of Tygon tubing containing a 3-way stopcock in between the flask and regulator where the third joint attaches to a Schlenk line. With the lecture bottle closed and regulator open and flask were evacuated and refilled with $Ar_{(g)}$ (10 cycles) and left under vacuum

following the last vacuum/$Ar_{(g)}$. The stopcock was turned such that the flask and regulator were connected to each other but closed to the Schlenk line. The regulator was then closed, and the lecture bottle opened until the regulator pressure stabilizes. The lecture bottle was then closed, and the regulator opened so that the volume of gas in the regulator would charge the evacuated flask. This was repeated until the pressure of the flask reached slightly above 1 atm. A 3-way gas tight syringe, pre-vacuum / $Ar_{(g)}$ purged and equipped with needle, was used to transfer the gas to a reaction vessel by drawing up gas from the flask headspace.

X-ray Crystallography

All reflection intensities were measured at 110 K using a SuperNova diffractometer (equipped with Atlas detector) with Mo *K*α radiation (λ = 0.71073 Å) under the program CrysAlisPro (Version CrysAlisPro 1.171.39.29c, Rigaku OD, 2017). The same program was used to refine the cell dimensions and for data reduction. The structure was solved with the program SHELXS-2018/3 (Sheldrick, 2018) and was refined on F^2 with SHELXL-2018/3 (Sheldrick, 2018). Numerical absorption correction based on gaussian integration over a multifaceted crystal model was performed using CrysAlisPro. The temperature of the data collection was controlled using the system Cryojet (manufactured by Oxford Instruments). The H atoms were placed at calculated positions using the instructions AFIX 23 or AFIX 137 with isotropic displacement parameters having values 1.2 or 1.5 U_{eq} of the attached C atoms. The structure is partly disordered.

The asymmetric unit contains one lattice THF solvent molecule that is disordered over three orientations. The sum of the occupancy factors were constrained to be 1, and the three occupancy factors refine to 0.509(2), 0.302(3) and 0.189(3).

1.2 Synthetic Methods

Preparation of $NO_{(g)}$ Saturated MeTHF, $NO_{(MeTHF)}$

In the glovebox ~3 mL of degassed MeTHF was drawn into a gastight syringe, with care taken to ensure no gas bubbles remained in the syringe barrel. The syringe needle was inserted into a rubber septum, and the syringe was removed from the glovebox. Outside of the glovebox the rubber septum was removed and ~0.5 mL of solvent was expelled, after which the remaining solvent was immediately injected into a Schlenk flask containing pre-purified $NO_{(g)}$. The MeTHF was allowed to equilibrate with the $NO_{(g)}$ for 30 min during which an oil bubbler with syringe needle attachment was sparged with $Ar_{(g)}$. After 30 min the oil bubbler syringe needle was inserted into the Schlenk flask containing the MeTHF and used to equilibrate the pressure of the flask with atmospheric pressure, giving a $NO_{(g)}$ saturated solution at ~1 atm, $NO_{(MeTHF)}$.

Determination of the NO(g) Concentration in $NO_{(MeTHF)}$, Titrations with $(F_8)Fe^{II}$

In the glovebox $[F_8Fe^{II}(H_2O)]$ was dissolved in 5 mL MeTHF ($[F_8Fe^{II}(H_2O)]$ = 8.2 μM based on Soret Absorption at 422 nm; ε_{422} = 210000) in a cuvette and sealed with rubber septum. $NO_{(MeTHF)}$ was titrated into this solution via a 10 μL syringe resulting in the conversion of $[F_8Fe^{II}(H_2O)]$ to $[F_8Fe^{II}(NO)]$.

Synthesis of $[Cu^{II}(TMG_2dien)(NO_2^-)]B(C_6F_5)_4$

The ligand TMG_2dien was prepared according to literature methods.[4] To a 250 mL round-bottom flask containing $Cu^{II}(OTf)_2$ (185.2 mg, 0.51 mmol) and $Cu^{II}(Cl)_2$ (68.3 mg, 0.51 mmol) and equipped with a stirbar, TMG_2dien (320.8 mg, 1.02 mmol) was added as a solution in 10 mL MeCN yielding a dark green solution. An additional 10 mL of MeCN was added to bring the total volume to 20 mL, and the solution was allowed to stir for 60 min. $AgNO_2$ (160.6 mg, 1.04 mmol) was added to the flask, under low light conditions, immediately turning the solution blue and turbid. The reaction was allowed to stir for an additional 15 minutes before the mixture was filtered through celite, and the filtrate concentrated under vacuum to give a dark blue oil. The oil was

dissolved in 20 mL THF, transferred to a 250 mL round-bottom flask and $KB(C_6F_5)_4$ (735.1 mg, 1.02 mmol) added. The mixture was allowed to stir for 60 min and subsequently filtered through Celite. To the filtrate, 200 mL of heptane was added yielding a light blue precipitate. The solid was collected over a medium porosity fritted glass funnel and dried on the vacuum line for 18h to give the title compound as a crude solid (1.1815 g). 200 mg of the solid was re-dissolved in ~ 3 mL of THF in a 20 mL scintillation vial and layered with hexanes, which over the course of several hours yielded x-ray quality deep blue plate-like crystals (134.8 mg, 65% overall yield). Elemental analysis: Calc. for $[Cu^{II}(TMG_2dien)(NO_2^-)]B(C_6F_5)_4 \bullet THF$ **(**$C_{43}H_{43}BCuF_{20}N_8O_3$): C 43.99, H 3.69, N 9.54; Found C 43.96, H 3.20, N 9.41.

Synthesis of $[Cu^{II}(TMG_3tren)(NO_2^-)]B(C_6F_5)_4$ via NO˙ Disproportionation

In the glovebox $[Cu^{I}(TMG_3tren)]B(C_6F_5)_4$ (113.7 mg, 0.096 mmol) was dissolved in 10 mL MeTHF and transferred to a 25 mL Schlenk flask. The flask was removed from the box and transferred to the Schlenk line where $NO_{(g)}$ (5 mL) was bubbled into the solution and the reaction was allowed to stir for 90 minutes changing from colorless to lime green. The solution was removed via vacuum and the solid was re-dissolved in Et_2O (~10 mL). After 15 minutes green needle like formed and were collected and dried under vacuum to give a lime green solid (66.0 mg, 55.9 % yield). Elemental analysis: Calc. for $[Cu^{II}(TMG_3tren)(NO_2^-)]B(C_6F_5)_4$ **(**$C_{45}H_{48}BCuF_{20}N_{11}O_2$): C 43.97, H 3.94, N 12.53; Found C 43.33, H 3.94, N 11.90.

Synthesis of $[Cu^{II}(TMG_3tren)(MeCN)](OTf)_2$

In the glovebox $Cu^{II}(OTf)_2$ (505.9 mg, 1.40 mmol) and TMG_3tren (614.2 mg, 1.39 mmol were dissolved in 10 mL MeCN in a 100 mL Schlenk flask yielding a bright green solution. The solution was allowed to stir for 60 minutes and then transferred to the Schlenk line and the solvent removed. The solid was re-dissolved in 10 mL of 1:4 MeCN:THF and Et_2O (40 mL) was added and after

stirring afforded a light green solid. The supernatant was decanted and the bright green solid washed with additional Et_2O (2 x 10 mL). The solid was then dried on the vacuum line and collected in the glovebox (815.7 mg, 70.0 % yield). Elemental analysis: Calc. for $[Cu^{II}(TMG_3tren)(MeCN)](OTf)_2$ **(**$C_{25}H_{51}BCuF_6N_{11}O_6S_2$): C 35.60, H 6.10, N 18.27; Found C 35.32, H 5.98, N 18.10.

1.3 Analytical Methods

Low Temperature UV Studies of $[Cu^{II}(TMG_3tren)(^{-}OONO)]B(C_6F_5)_4$ Using $NO_{(MeTHF)}$

In a typical experiment $[Cu^{I}(TMG_3tren)]B(C_6F_5)_4$ (2.4 mg, 0.002 mmol) was dissolved in 10 mL of MeTHF in an inert atmosphere glovebox. 2.5 mL of this solution was syringed into a Schlenk cuvette transferred the UV-cryostat precooled to –125 ºC. The solution was bubbled with $O_{2(g)}$ through a syringe needle directly to an O_2 gas tank (regulator pressure ~ 10 PSI) and vented out through a second needle, for 20 s to generate the superoxide complex, $[Cu^{II}(TMG_3tren)(O_2^{\bullet-})]B(C_6F_5)_4$. Excess O_2 was then removed via sparging the solution with $Ar_{(g)}$ for 2 minutes and performing vacuum argon purge cycles (10 cycles). $NO_{(MeTHF)}$ (0.17 mL, ~7 eq) was added via syringe. Over the course of 30 min $[Cu^{II}(TMG_3tren)(O_2^{\bullet-})]B(C_6F_5)_4$ was fully converted to $[Cu^{II}(TMG_3tren)(^{-}OONO)]B(C_6F_5)_4$.

Job's Plot Analysis of the EPR Data

In the glovebox $[Cu^{I}(TMG_3tren)]B(C_6F_5)_4$ (23.3 mg, 0.02 mmol) was dissolved in 10 mL of MeTHF. An appropriate volume of LCu^{I} solution and MeTHF solvent was added to EPR tubes such that the total volume after $NO_{(MeTHF)}$ addition was 0.5 mL and the total moles of LCu^{I} + NO = 1 μmol. The samples were sealed with rubber septa and parafilm and transferred out of the glovebox to a liquid nitrogen / pentane bath (–130 ºC). O_2 was bubbled through the solution for 30 s allowed to react for 5 min before and $Ar_{(g)}$ was sparged through the solution to remove excess

O_2. The requisite amount of $NO_{(MeTHF)}$ was then added and the reaction was allowed to incubate for 60 minutes before freezing in liquid nitrogen.

Nitrite Assay of the Reaction Products

In the glovebox a 10 mL Schlenk Flask equipped with stirbar was charged with 11.5 mg of $[Cu^{I}(TMG_3tren)]B(C_6F_5)_4$ dissolved in 10 mL MeTHF (0.97 mM) and sealed with a rubber septum. The flask was taken out the glovebox and placed in a liquid nitrogen / pentane cooling bath (–130 ºC). O_2 was bubbled through the cooled solution for 30 s to generate $[Cu^{II}(TMG_3tren)(O_2^{\bullet-})]B(C_6F_5)_4$ as an emerald green solution. $Ar_{(g)}$ was bubbled through the solution to remove excess O_2 and $NO_{(g)}$ was injected via a 3-way gastight syringe. The reaction was allowed to run 60 min resulting in a change in the solution from emerald green to colorless. $Ar_{(g)}$ was again bubbled through the solution and vacuum argon purge cycles applied to remove excess $NO_{(g)}$. The reaction was allowed to warm up to room temperature giving a blue-tinted green solution. The solvent was then removed and the resulting solid re-dissolved in 3 mL of dichloromethane. The dichloromethane solution was extracted three times with 3, 3, and 4 mL of $NaCl_{(aq)}$ (20 mM). The combined aqueous phases were tested for nitrite via the Griess Assay (Molecular Probes Griess Reagent Kit; ThermoFisher G7921), and referenced against authentic $[Cu^{II}(TMG_3tren)(NO_2^{-})]B(C_6F_5)_4$.

Spin Trapping using DMPO

In the glovebox 2.5 mL of 0.21 mM $[Cu^{I}(TMG_3tren)]^{+}$ solution was added to a cuvette and sealed with a rubber septum and parafilm. The cuvette was transferred to a cryostat cool to –125 ºC, and **PN1** was generated as described above. Following full formation of **PN1** $Ar_{(g)}$ was sparged through the solution for 2 minutes, followed by vacuum $Ar_{(g)}$ cycles (10 cycles). DMPO (500 equiv) was added and allowed incubate for 30 min; no reaction was observed. The mixture was warmed to

room temperature yielding a faint green solution. The solvent was removed on the vacuum line taking care not to expose the solution to air by vacuum / Ar purging the cuvette side arm before placing the solution under vacuum. Once all the solvent was removed, the residue re-dissolved in ~3 mL MeCN and the mixture was analyzed via ESI-MS.

Gas Chromatography Analysis of Phenolic Products from PN1 Decomposition

In a Schlenk cuvette at –125 ºC **PN1** (2.5 mL, 0.15 mM) was formed and 2,4-DTBP (125 μL, 530 equiv) was added via syringe (minimal reaction observed over the course of 10 minutes). Following 10 minutes the cuvette was warmed to room temperature and the solvent removed. The residue was re-dissolved in 0.9 mL methanol and 0.1 mL of $C_{12}H_{26}$ (12.3 mM in methanol) was added as an internal standard (final $C_{12}H_{26}$ concentration = 1.23 mM). 2 μL of this solution was injected into the GC with FID detector using the following instrument conditions: Oven: 120 ºC (2 min), ramp 30 ºC / min to 200 ºC, 200 ºC (5 min), ramp 30 ºC / min 250 ºC, 250 ºC (5 min); Inlet: (250 ºC); Detector (300 ºC); Column flow rate: (1.8 mL / min).

2. Job's Plot Generated via EPR Spectroscopy

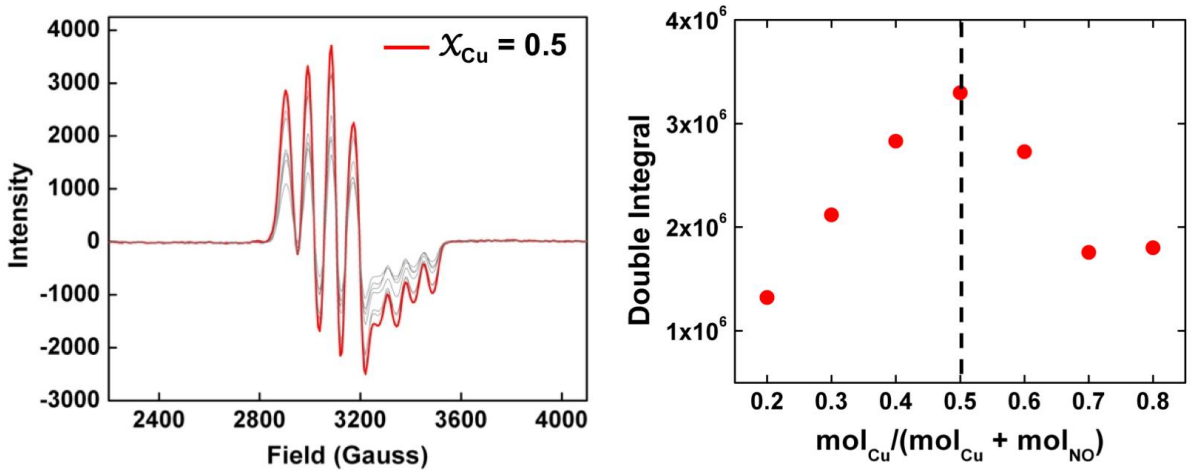

Figure S1 (Left) EPR spectra of various mol. ratios (0.2 – 0.8) of $[Cu^{II}(TMG_3tren)(O_2^{\bullet-})]^+$ and $NO_{(MeTHF)}$. (**Right**) Job's plot showing maximal formation of **PN1** occurs when the mol. ratio of $[Cu^{II}(TMG_3tren)(O_2^{\bullet-})]^+$ to $NO_{(MeTHF)}$ is 1:1. Total Cu + NO concentration = 1 μmol.

3. Resonance Raman Spectra of Isotopically Labeled PN1

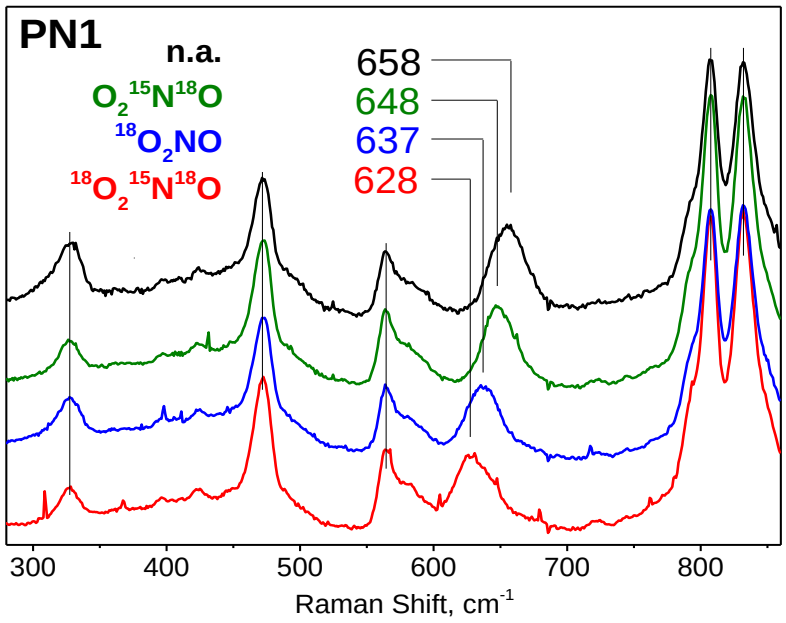

Figure S2. Resonance Raman spectra of **PN1** (407 nm excitation) generated from natural abundance (n.a.) O_2 and NO (black), n.a. O_2 and $^{15}N^{18}O$ (green), $^{18}O_2$ and n.a. NO (blue), and $^{18}O_2$ and $^{15}N^{18}O$ (red).

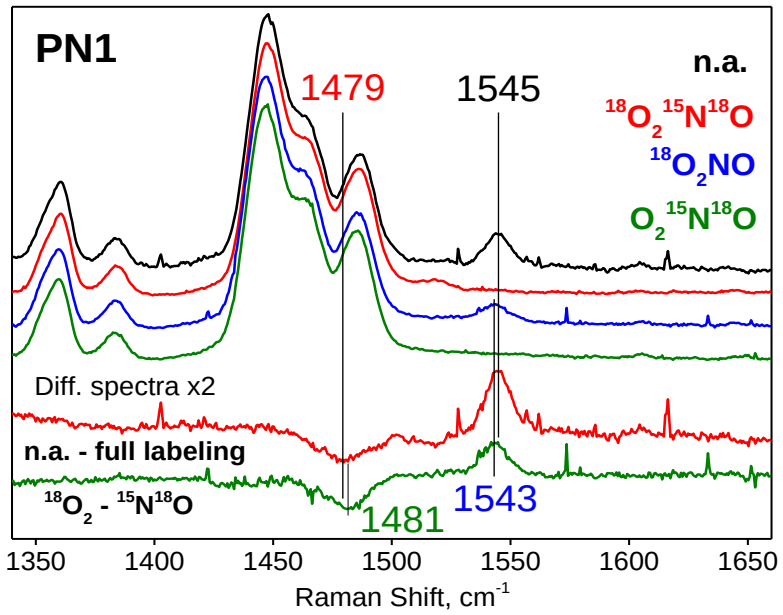

Figure S3. Resonance Raman spectra of **PN1** (407 nm excitation) generated from natural abundance (n.a.) O_2 and NO (black), $^{18}O_2$ and $^{15}N^{18}O$ (red), $^{18}O_2$ and n.a. NO (blue), and n.a. O_2 and $^{15}N^{18}O$ (green); also shown are difference spectra isolating the isotope sensitive Raman signals.

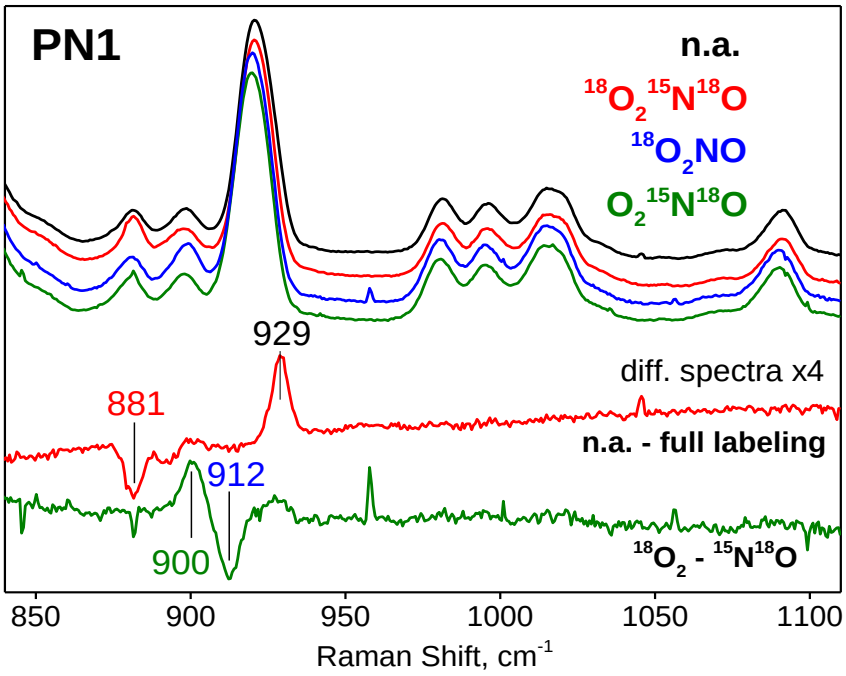

Figure S4. Resonance Raman spectra of **PN1** (407 nm excitation) generated from natural abundance (n.a.) O_2 and NO (black), $^{18}O_2$ and $^{15}N^{18}O$ (red), $^{18}O_2$ and n.a. NO (blue), and n.a. O_2 and $^{15}N^{18}O$ (green); also shown are difference spectra isolating the isotope sensitive Raman signals.

4. Selected Metrical Parameters for the Calculated Structure for *cis* and *trans*-PN1

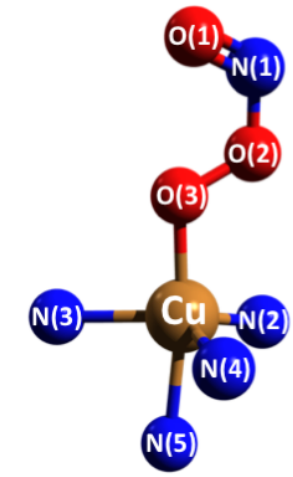

τ = 0.90

Distance (Å)			Angle (°)
Cu-N(2)	2.117	N(2)-Cu-O(3)	104.0
Cu-N(3)	2.128	N(2)-Cu-N(3)	118.5
Cu-N(4)	2.128	Cu-O(3)-O(2)	114.6
Cu-N(5)	2.153	O(2)-Cu-N(5)	172.5
Cu-O(3)	1.957		
O(3)-O(2)	1.409	O(3)-O(2)-N(1)-O(1)	0.4
O(2)-N(1)	1.370	Cu-O(3)-O(2)-N(1)	−174.4
N(1)-O(1)	1.188	Cu-O(2)-N(1)-O(1)	−7.3

Figure S5 Optimized geometry and selected metrical parameters for *cis*-**PN1** An initial guess geometry derived from the X-ray crystal structure for $[Cu^{II}(TMG_3tren)(O_2^{\bullet-})]SbF_6$. Optimization was performed at the b3lyp level of theory using the spin unrestricted formulism, and the D3 dispersion correction. Def2-TZVP was used as the basis set for all atoms. The polarizable continuum model (PCM) using the THF parameters was used to model MeTHF solvation. $\tau = 0.90$, where $\tau = 0$ for a perfect square pyramidal geometry and $\tau = 1$ is perfect trigonal bipyramidal geometry.[5]

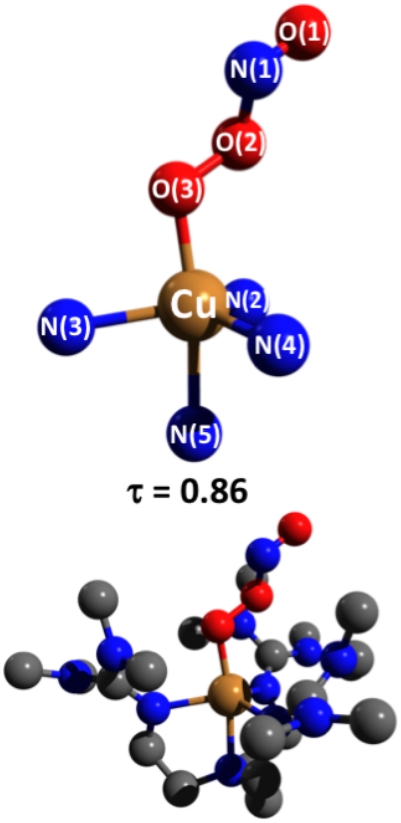

Distance (Å)			Angle (°)
Cu-N(2)	2.119	N(2)-Cu-O(3)	102.5
Cu-N(3)	2.116	N(2)-Cu-N(3)	120.3
Cu-N(4)	2.155	Cu-O(2)-O(3)	113.4
Cu-N(5)	2.155	O(3)-Cu-N(5)	171.8
Cu-O(3)	1.948		
O(3)-O(2)	1.415	O(3)-O(2)-N(1)-O(1)	−178.1
O(2)-N(1)	1.370	Cu-O(3)-O(2)-N(1)	−144.5
N(1)-O(1)	1.192	Cu-O(2)-N(1)-O(1)	148.6

Figure S6 Optimized geometry and selected metrical parameters for *trans*-**PN1** An initial guess geometry derived from the X-ray crystal structure for $[Cu^{II}(TMG_3tren)(O_2^{\bullet-})]SbF_6$. Optimization was performed at the b3lyp level of theory using the spin unrestricted formulism, and the D3 dispersion correction. Def2-TZVP was used as the basis set for all atoms. The polarizable continuum model (PCM) using the THF parameters was used to model MeTHF solvation. $\tau = 0.05$, where $\tau = 0$ for a perfect square pyramidal geometry and $\tau = 1$ is perfect trigonal bipyramidal geometry.[5]

5. Calculated Raman Spectra for *cis* and *trans*-PN1

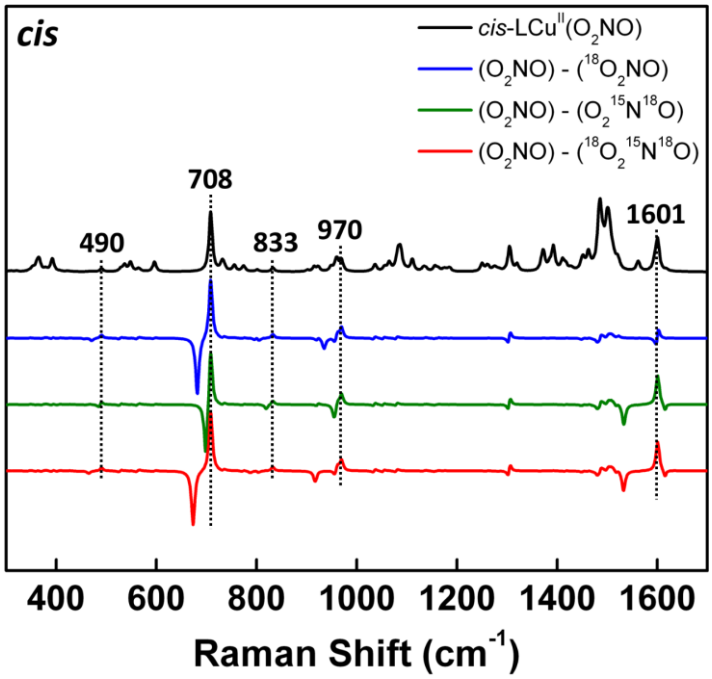

Figure S7 Analytical Raman spectra and difference spectra of *cis*-**PN1** and its isotopologues (8 cm^{-1} Gaussian broadening) calculated using the optimized structure in **Figure S5**.

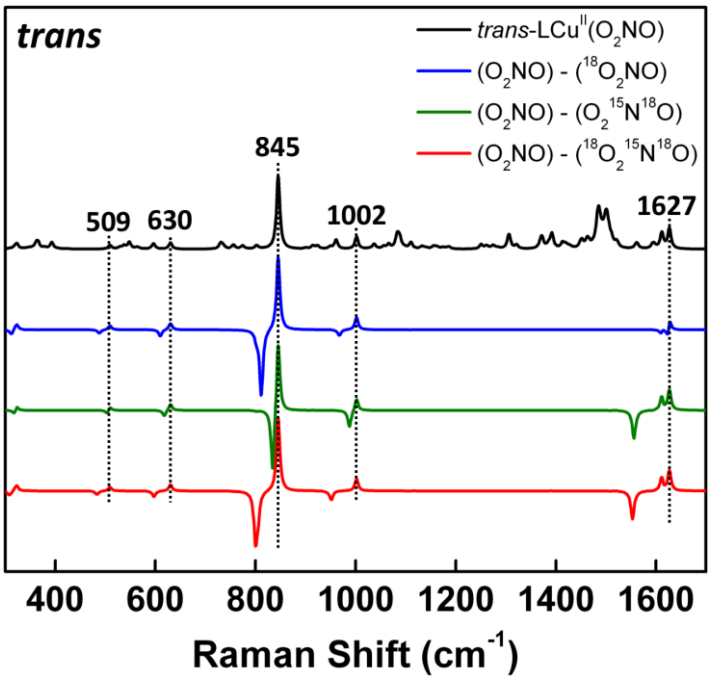

Figure S8 Analytical Raman spectra and difference spectra of *trans*-**PN1** and its isotopologues (8 cm^{-1} Gaussian broadening) calculated using the optimized structure in **Figure S6**.

6. Peroxynitrite Vibrations in *cis*-PN1 (left) and *trans*-PN1 (right)

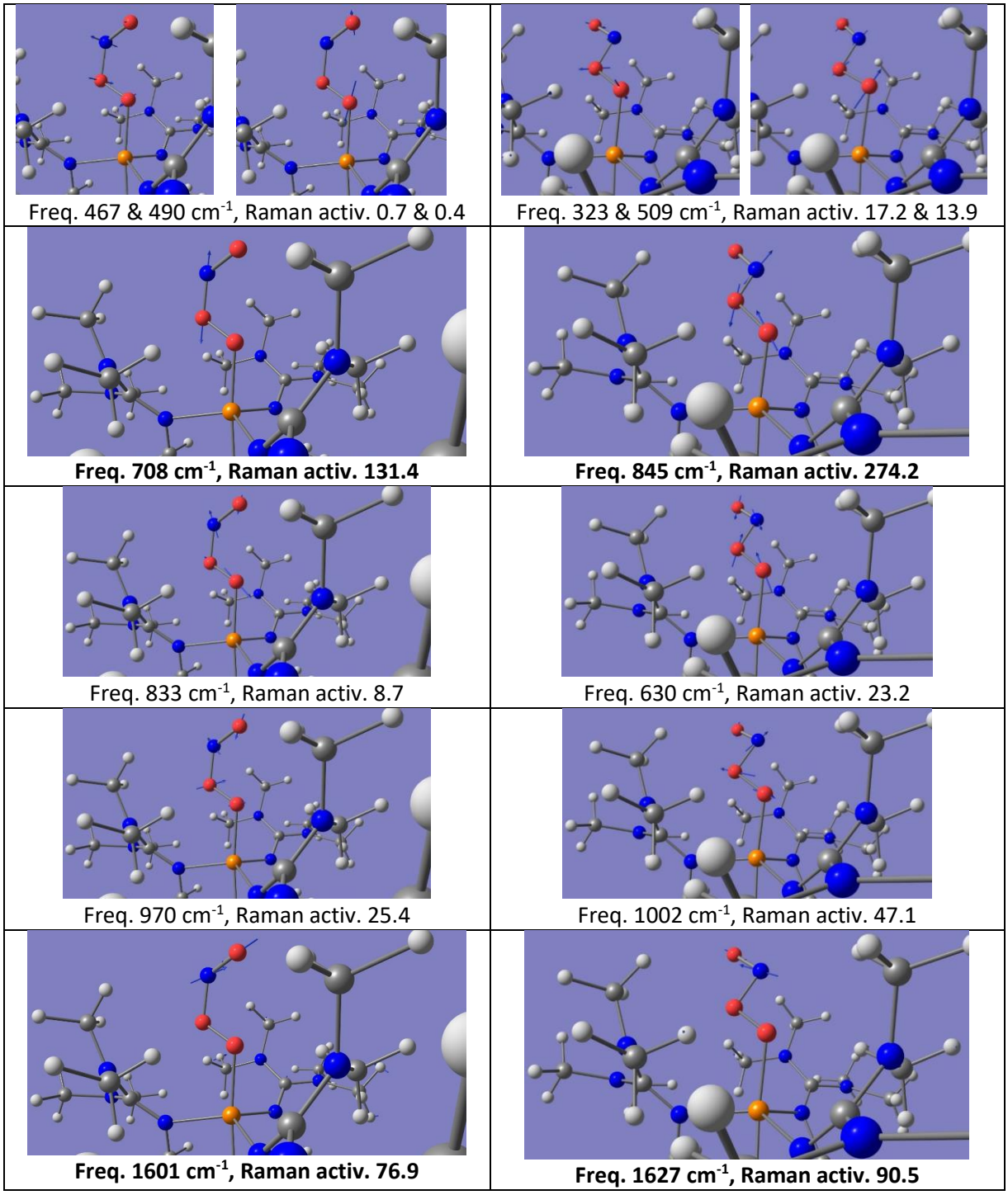

Figure S9 Calculated normal mode eigenvectors for the *cis* (**left**) and *trans* (**right**) PN structures.

7. Fitted EPR Spectra of PN1 and PN2

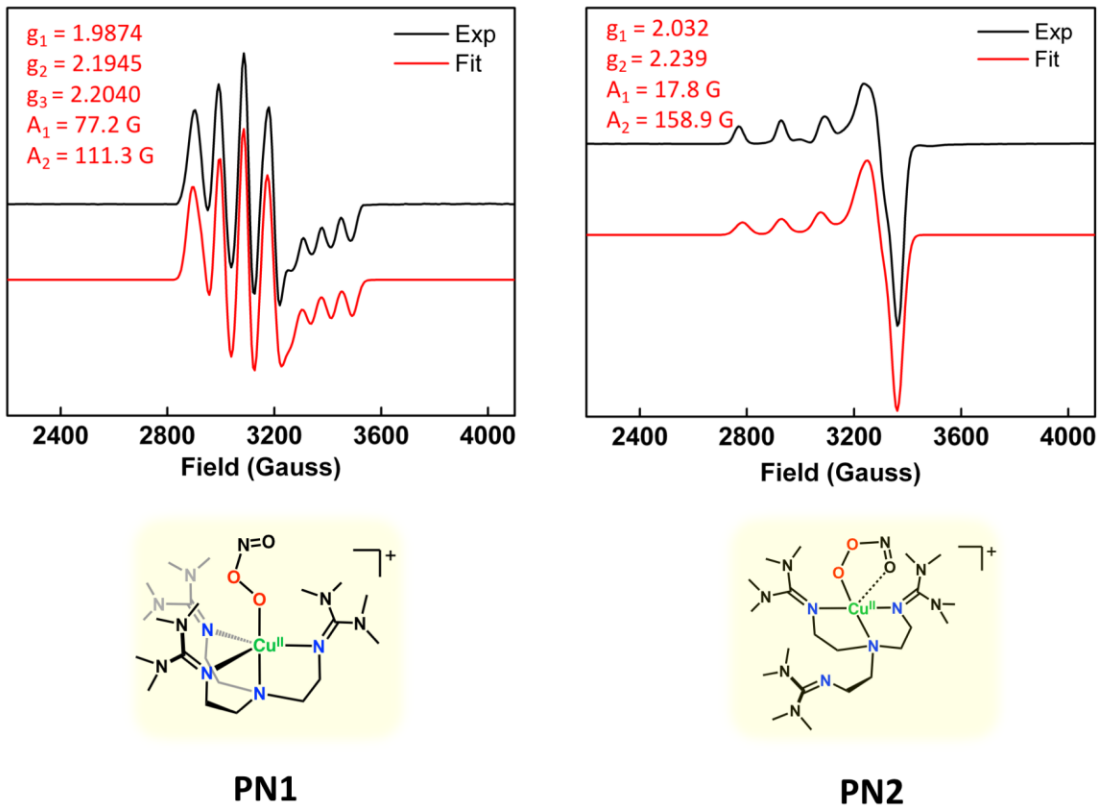

Figure S10 Fitted EPR spectra of **PN1** (generated at –130 ºC) and **PN2** (generated at –80 ºC) Using EasySpin software package in MatLab.

8. ESI-MS Spectrum of $[Cu^{II}(TMG_3tren)(OONO)]^+$ Warm up Product Mixture

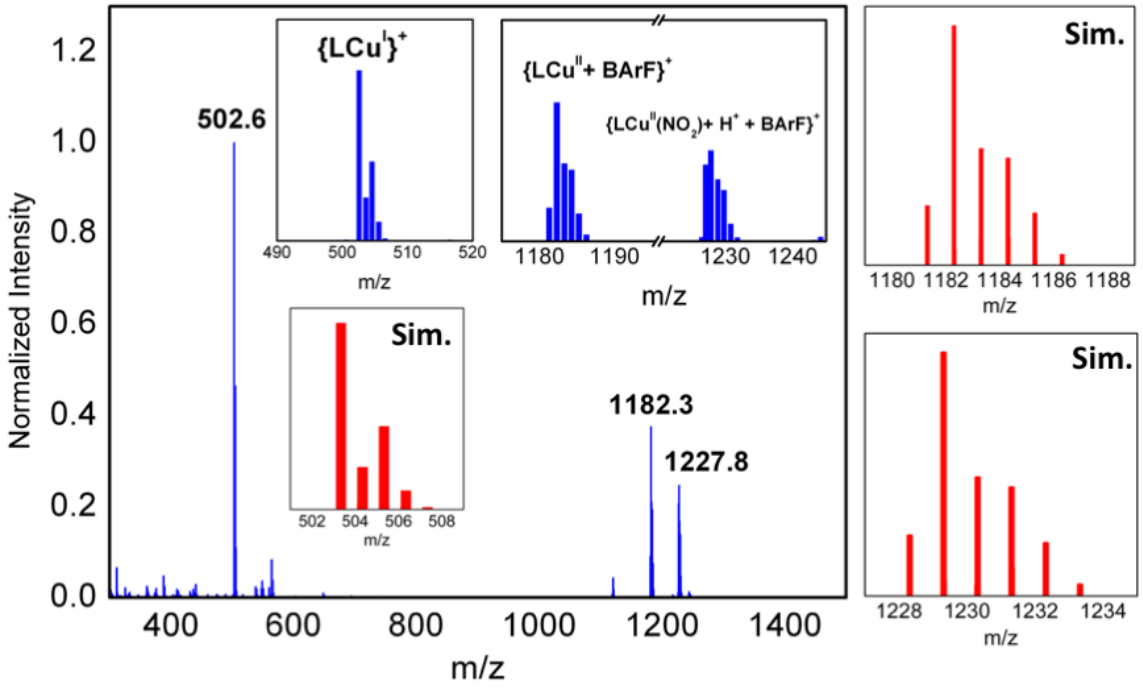

Figure S11 ESI-MS spectrum (blue) of the warm up mixture from the decomposition of **PN1**. The red spectra show the simulated theoretical isotope distribution patterns for $\{LCu^{I}\}^+$, $\{LCu^{II} + BArF^-\}^+$, and $\{LCu^{II}(NO_2^-) + H^+ + BArF^-\}^+$. $BArF^- = B(C_6F_5)_4^-$.

9. EPR Spectra of PN2 and $[Cu^{II}(TMG_3tren)(\kappa^2\text{-}O,O'\text{-}NO_2)]^+$

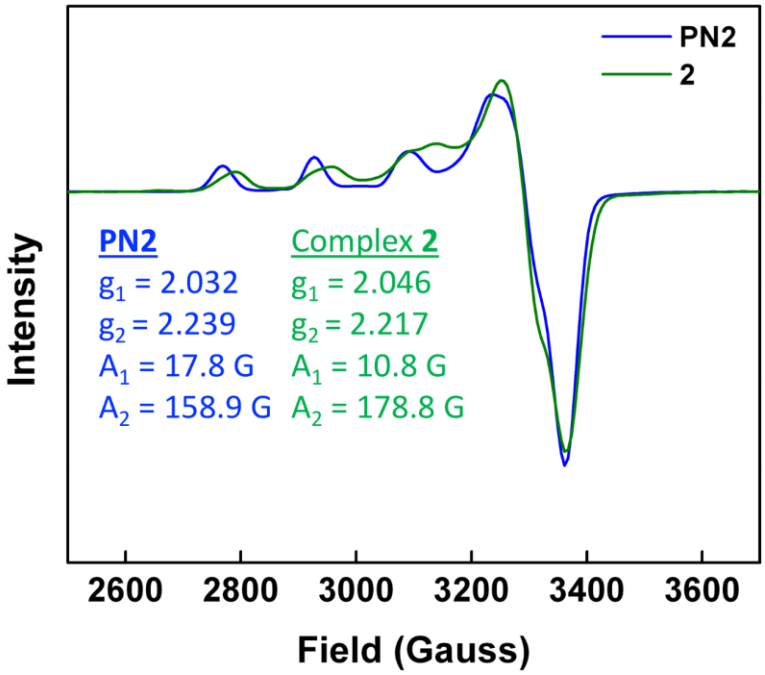

Figure S12 EPR spectrum (MeTHF, 20K) and fitted EPR parameters for **PN2** (blue) and the warm up copper-nitrite complex (**2**, green), likely possessing a de-ligated ligand arm.

10. $[Cu^{II}(TMG_2dien)(\kappa^2\text{-}O,O'\text{-}NO_2^-)]B(C_6F_5)_4$ X-ray Structure Selected Parameters

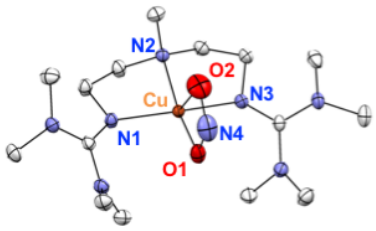

$\tau = 0.05$

Distance (Å)			Angle (°)
Cu-N(1)	1.963	O(1)-Cu-N(2)	165.14
Cu-N(2)	2.033	N(1)-Cu-N(3)	162.41
Cu-N(3)	1.956	N(1)-Cu-N(2)	84.47
Cu-O(1)	1.993	N(1)-Cu-O(1)	99.67
Cu-O(2)	2.456	N(1)-Cu-O(2)	104.20
		N(2)-Cu-N(3)	84.78
		O(2)-Cu-N(2)	109.69
		O(2)-Cu-N(3)	92.53
		O(1)-Cu-N(3)	94.25

Figure S13 X-ray crystal structure (ORTEP 50% probability, hydrogens omitted for clarity) for $[Cu^{II}(TMG_2dien)(\kappa^2\text{-}O,O'\text{-}NO_2^-)]B(C_6F_5)_4$, and selected metical parameters. $\tau = 0.05$, where $\tau = 0$ for a perfect square pyramidal geometry and $\tau = 1$ is perfect trigonal bipyramidal geometry.[5]

11. UV-vis and EPR Spectroscopy Characterization of $[Cu^{II}(TMG_2dien)]^+$

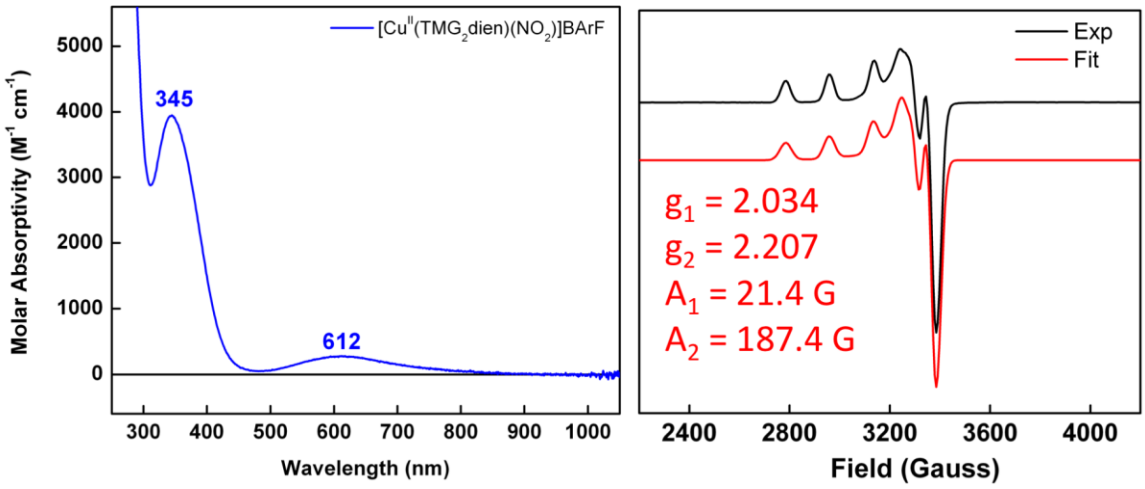

Figure S14 UV-vis and EPR spectra (and corresponding fitted EPR parameters) of independently synthesized $[Cu^{II}(TMG_2dien)(\kappa^2\text{-}O,O'\text{-}NO_2^-)]^+$ (see experimental for synthetic details) in MeTHF. EPR spectra collected at 20 K as a frozen solution.

12. UV-vis quantitation of Cu^{II}-NO_2 Yield

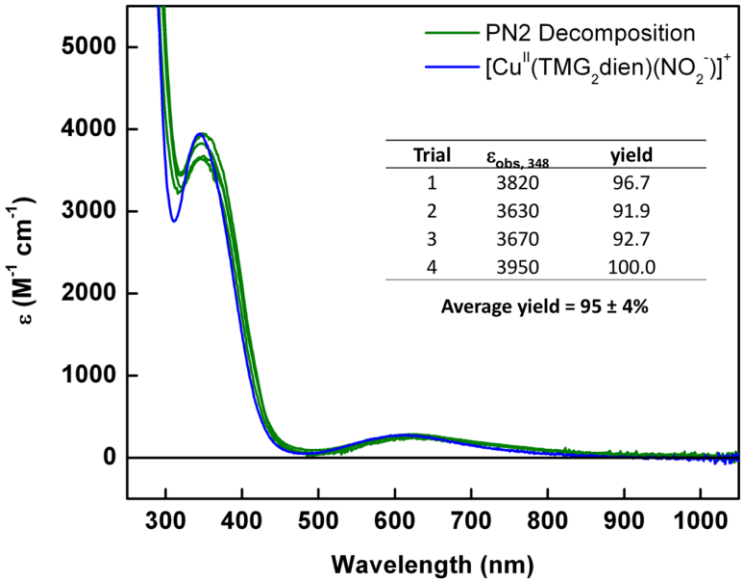

Figure S15 Spectrophotometric yields of $[Cu^{II}(TMG_3tren)(\kappa^2\text{-}O,O'\text{-}NO_2)]^+$ from decay of **PN2**. Yields are based off the absorptivity determined for the complex's charge transfer band compared to $Cu^{II}(TMG_2dien)(\kappa^2\text{-}O,O'\text{-}NO_2)]^+$ (ε_{345} = 3950 M^{-1} cm^{-1}).

13. Nitrite (Griess) Assay

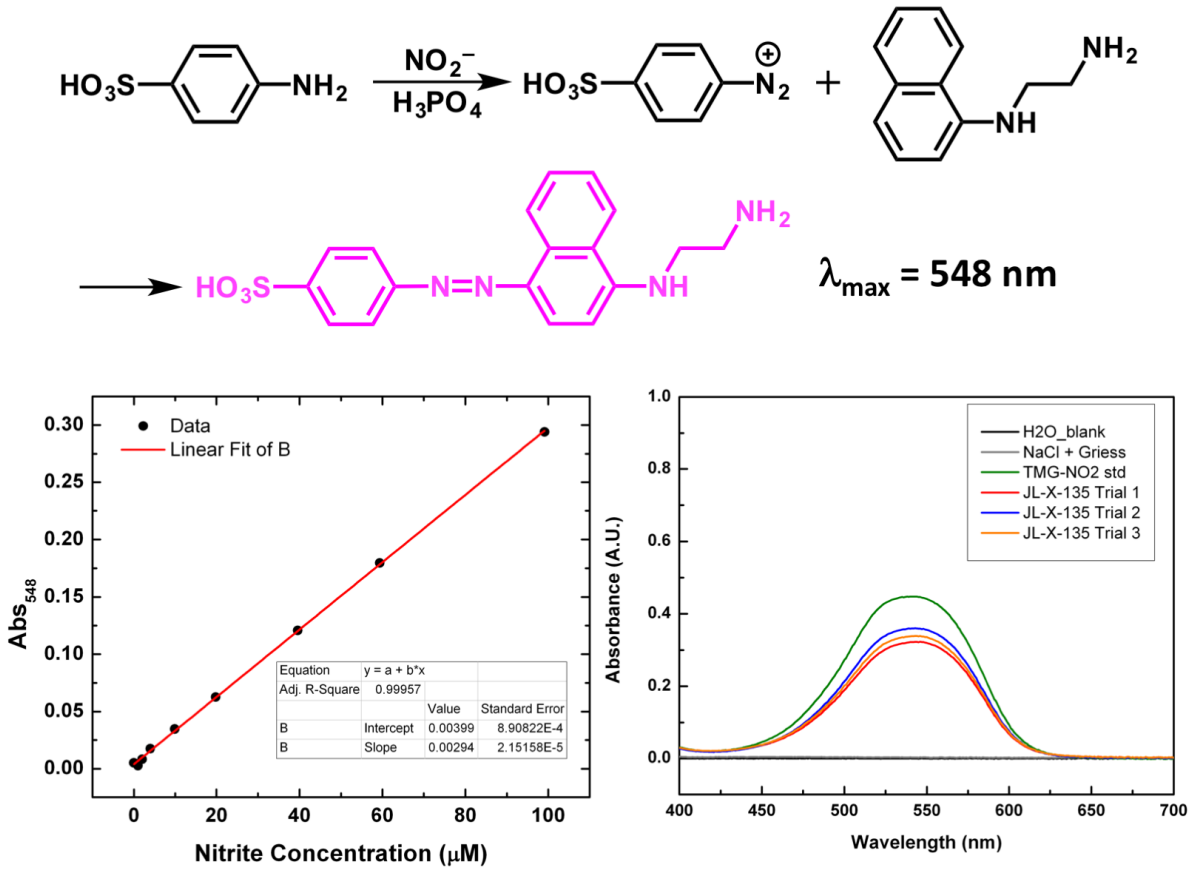

Figure S16 (**Top**) ChemDraw scheme depicting the formation of the diazonium dye used in the Griess nitrite quantification assay. (**Bottom, Left**) Calibration curve created using $NaNO_2$. (**Bottom, Right**) Representative UV-vis of the assay monitoring formation of the diazonium dye at 548 nm.

sample	Abs(548)	conc (uM) NO_2^-	conc Cu (uM)	% Yield (NO_2)	% Yield (Cu-NO_2)
Trial 1	0.30	590.9	971.9	60.8	78.7
Trial 2	0.27	522.8	971.9	53.8	69.6
Trial 3	0.26	512.7	971.9	52.8	68.2
				Average	**72.2**

sample	Abs(548)	conc (uM) NO_2^-	conc Cu (uM)	% Yield(NO_2)	% Yield (Cu-NO_2)
Trial 1	0.41	811.2	980.3	82.7	78.7
Trial 2	0.42	825.5	980.3	84.2	80.1
Trial 3	0.36	702.8	980.3	71.7	68.2
				Average	**75.6**

sample	Abs(548)	conc (uM) NO_2^-	conc Cu (uM)	% Yield(NO_2)	% Yield (Cu-NO_2)
Trial 1	0.32	632.3	1031.0	61.3	71.8
Trial 2	0.36	706.1	1031.0	68.5	80.1
Trial 3	0.34	663.0	1031.0	64.3	75.2
				Average	**75.7**

Table S1 Tabulation of Cu-nitrite yields from $[Cu^{II}(TMG_3tren)(OONO)]^+$ (**PN2**) decay via the Griess Assay. Reported Cu-nitrite yields are normalized *vs*. determinations made for an authentic $[Cu^{II}(TMG_3tren)(NO_2^-)]B(C_6F_5)_4$ complex prepared from the method of $NO^\bullet$ disproportionation by $[Cu^{I}(TMG_3tren)]\ B(C_6F_5)_4$.

14. Kinetic Fits of $[Cu^{II}(TMG_3tren)(\kappa^2\text{-}O,O'\text{-}NO_2)]^+$ Formation from PN2 Decomposition

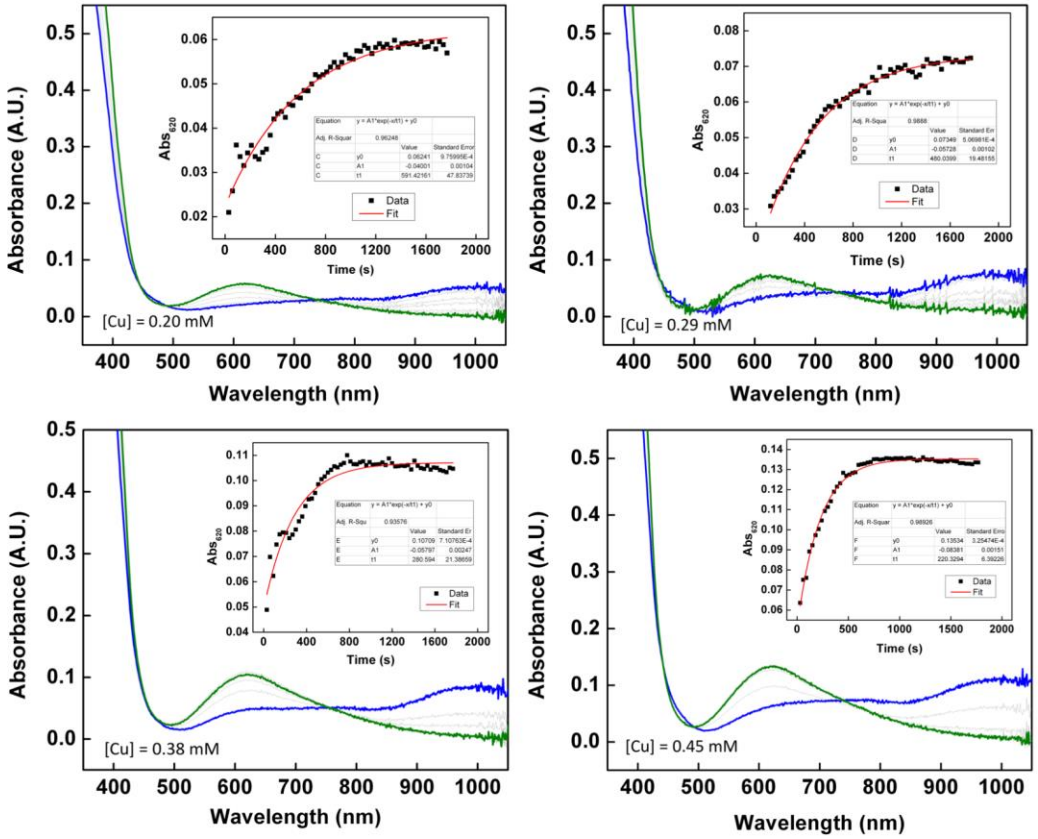

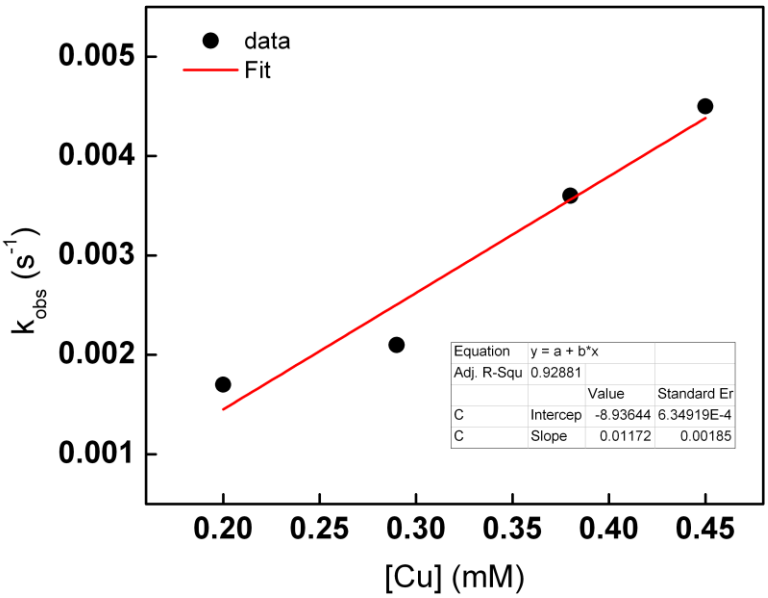

Figure S17 (**Top**) UV-vis spectra (top four panels) and time traces (insets) of $[Cu^{II}(TMG_3tren)(\kappa^2\text{-}O,O'\text{-}NO_2)]^+$ formation from PN2 decomposition at –60 ºC; Formation rates of $[Cu^{II}(TMG_3tren)(\kappa^2\text{-}O,O'\text{-}NO_2)]^+$ as a function of copper concentration support a first-order dependence in copper in the order of 10 $M^{-1}s^{-1}$ (bottom panel).

15. Proposed Mechanism for PN1 Decomposition in the Absence of Substrate

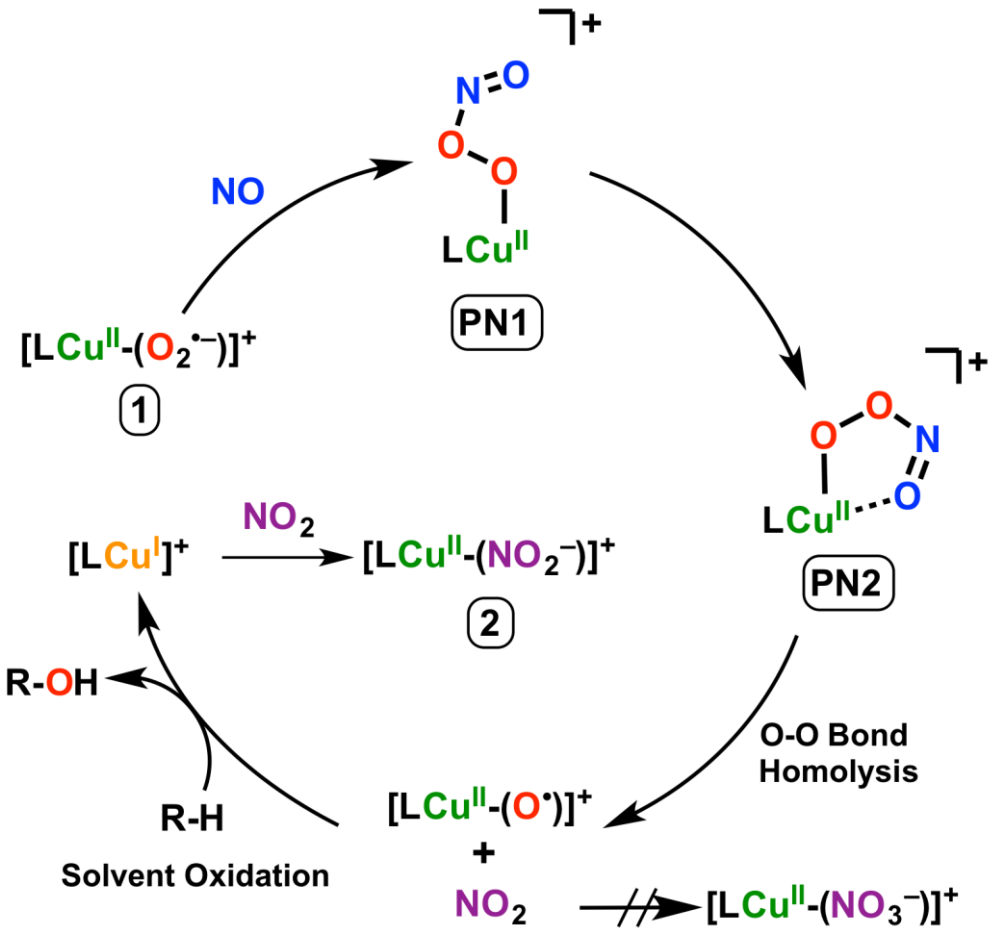

Scheme S1 Proposed reaction mechanism for the decomposition of **PN1** in the absence of substrate to give complex **2**. Our previous studies postulated that the cupryl intermediate attacks a second **PN2**, ultimately yielding ½ equiv of O_2 per copper peroxynitrite (Scheme S2).[6] Renewed efforts to detect the formation of O_2 from **PN2** were unsuccessful (Figure S21), thus we now favor a reaction mechanism where the highly reactive $[Cu^{II}(TMG_3tren)(O^{\bullet})]^+$ intermediate hydroxylates the solvent MeTHF in a radical rebound type mechanism (R–H = MeTHF). This hypothesis is predicated on the known reactivity of metal oxygen complexes ability to oxidize THF to 2-hydroxytetrahydrofuran (2-OH-THF) as has been demonstrated for several Cu_2^I/O_2 derived species.[7,8]. The resulting LCu^I complex formed after substrate hydroxylation is subsequently oxidized by $NO_2^{\bullet}$ to yield the nitrito complex **2**.

16. Scheme of Copper and Metal Mediated Peroxynitrite Decomposition Pathways which Yield Metal-Nitrito Species

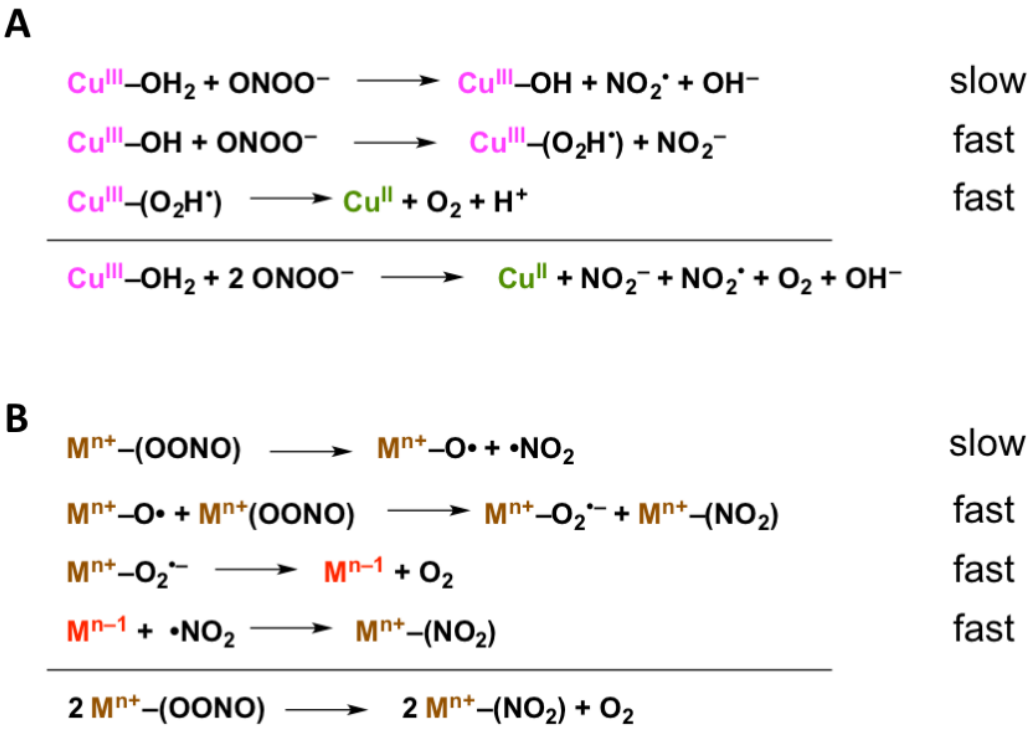

Scheme S2 (**A**) Copper catalyzed peroxynitrite decomposition under alkaline aqueous conditions. The $Cu^{III}–OH_2$ intermediate is postulated to be generated from $OH^{\bullet}$ and $Cu^{II}–OH_2$. (**B**) Decay of $M^{n+}–OONO$ in organic media, as deduced from studies of transition metal peroxynitrite chemistry. Homolysis of the O–O bond generates a $M^{n+}–O\bullet$ (or $M^{n+1}=O$) intermediate, which oxidizes a second equivalent of $M^{n+}–OONO$ to ultimately yield 2 $M^{n+}–NO_2$ and O_2.

17. Gas Chromatography of 2,4-di-*tert*-butylphenol Oxidation Products by PN1 Decay

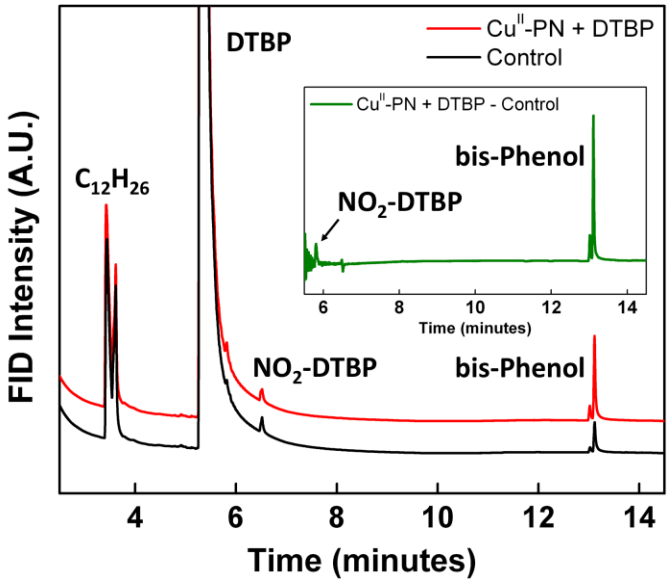

Figure S18 GC chromatogram of the reaction mixture following addition of 530 equivalents of 2,4-DTBP to a solution of **PN1** (red). A GC chromatogram of a control reaction without adding copper complex, but still adding and removing O_2 / NO (black). The main oxidized phenol product is the bis-phenol product 3,3',5,5'-tetra-*tert*-butyl-[1,1'-biphenyl]-2,2'-diol (>95% yield). Nitrated phenol, (6-nitro-2,4-di-tert-butylphenol) was also observed as a minor product (~5 %). Dodecane (1.2 mM) is present as an internal standard.

18. UV-vis Spectra of the Reaction of PN1 with 2,4-di-*tert*-butylphenol

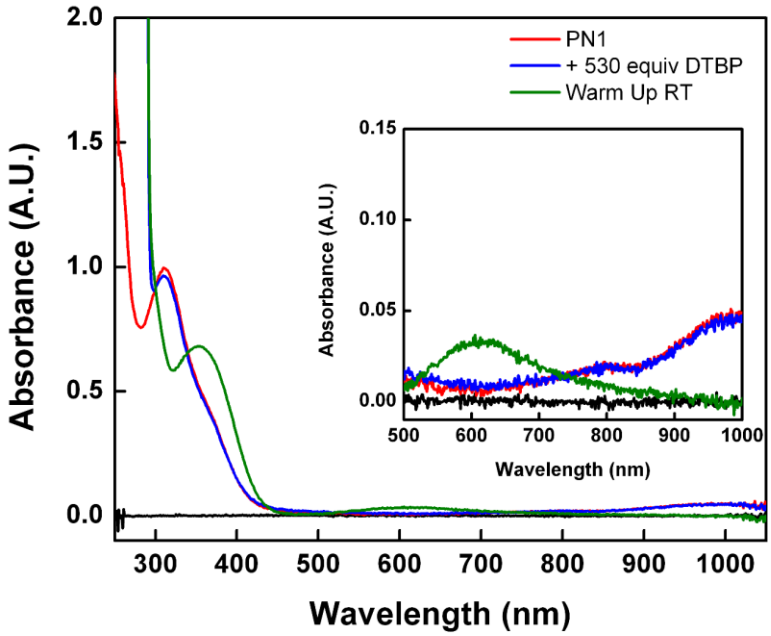

Figure S19 Addition of 530 equiv DTBP to **PN1** (0.15 mM) results in no reaction at –125 ºC. Warming the reaction mixture up to R.T. affords the $[Cu^{II}(TMG_3tren)(\kappa^2\text{-}O,O'\text{-}NO_2^-)]^+$ complex in quantitative yield.

19. ESI-MS of Spin Trap Reaction with DMPO

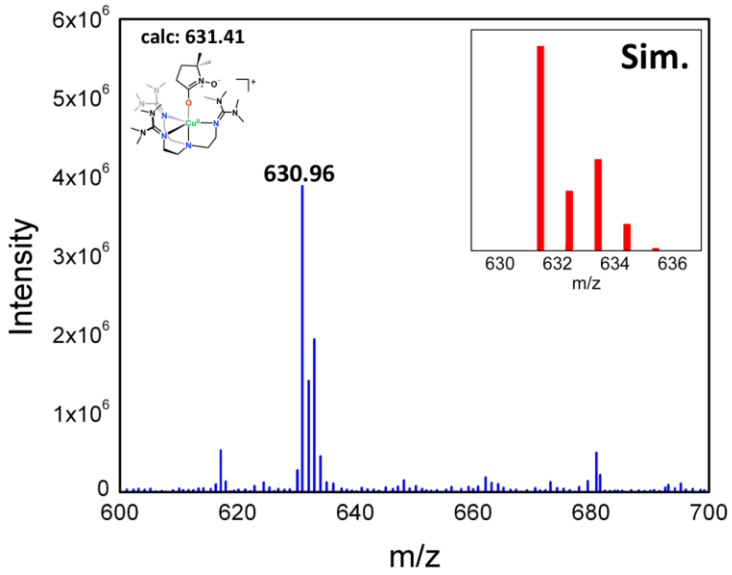

Figure S20 ESI-MS spectrum of the room temperature reaction mixture following addition of 500 eq. DMPO to **PN1** at –125 ºC. (Inset) Simulated isotope distribution pattern for $\{LCu^{II}(O–DMPO)\}^{+}$.

20. O_2 Quantification via Addition of $[Cu^{I}(TMG_3tren)]^{+}$

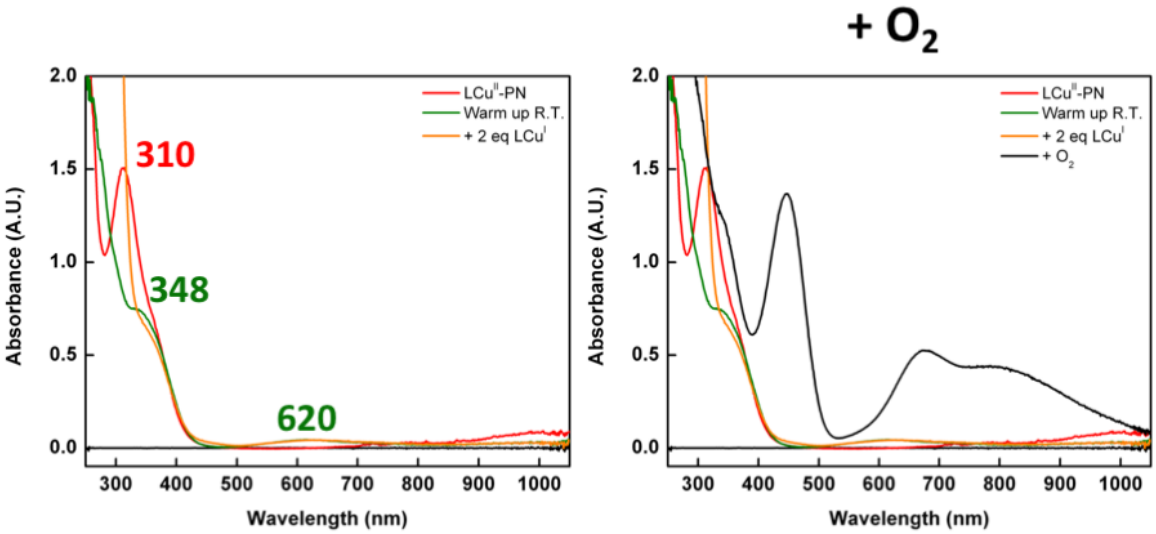

Figure S21 $[Cu^{II}(TMG_3tren)(OONO)]^{+}$ (0.2 mM) was generated at –125 ºC in MeTHF (red) allowed to warm to room temperature before cooling back down to –125 ºC (green). 2 equiv of cuprous complex $[Cu^{I}(TMG_3tren)]^{+}$ was added (orange) via syringe to test for possible O_2 generation of a well-known adduct $[Cu^{II}(TMG_3tren)(O_2^{\bullet-})]^{+}$. No O_2 was detected and the cupric superoxide complex was not detected until exogenous O_2 was sparged into solution giving authentic $[Cu^{II}(TMG_3tren)(O_2^{\bullet-})]^{+}$ spectrum (black).

21. Gas Chromatography Calibration Curves of Phenol Reaction Products

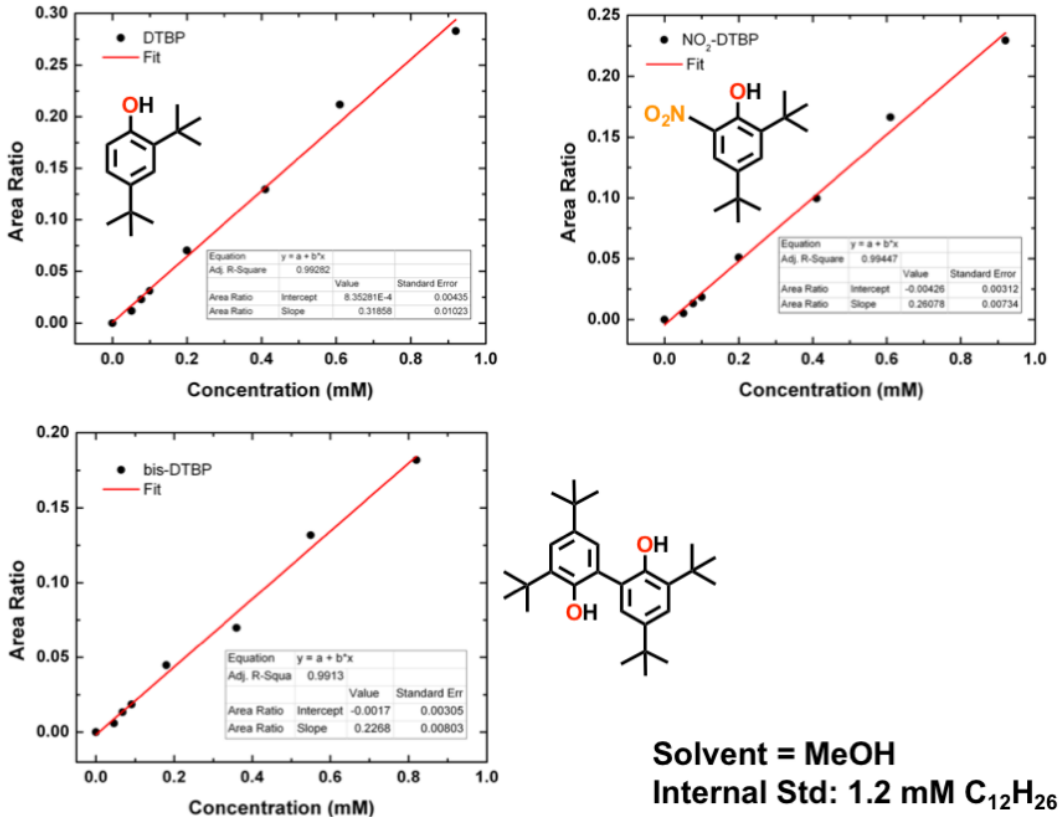

Figure S22 GC calibration curve of 2,4-di-*tert*-butylphenol, 6-nitro-2,4-di-*tert*-butylphenol, and 3,3',5,5'-tetra-*tert*-butyl-[1,1'-biphenyl]-2,2'-diol. Area ratio is calculated as: area analyte peak / area internal standard.

22. Reaction of $[Cu^{II}(TMG_3tren)(OH)]^+$ with 2,4-di-*tert*-butylphenol

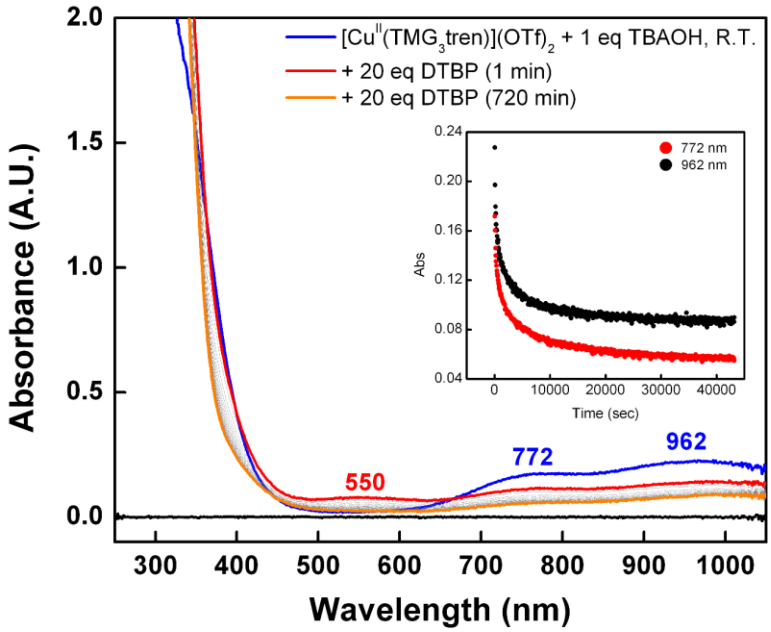

Figure S22 UV-vis spectra following the reaction of $[Cu^{II}(TMG_3tren)(OH)]^+$ (blue) (generated from addition of $[Cu^{II}(TMG_3tren)(MeCN)]^{2+}$ with NBu_4OH in an 1:1 ratio) with 20 equiv DTBP in 2% MeOH in THF after 12 hours under N_2 at room temperature. Use of 2% MeOH in THF was necessary to solubilize the initial $[Cu^{II}(TMG_3tren)(MeCN)]^{2+}$ complex. This result indicates LCu^{II}–OH reacts with DTBP only slowly, which is why we propose that it is $NO_2^{\bullet}$, as a strong oxidant which effects formation of the 2nd equiv of 2,4-di-tert-butylphenoxyl radical.

23. Titration of $[F_8Fe^{II}(H_2O)]$ with $NO_{(MeTHF)}$

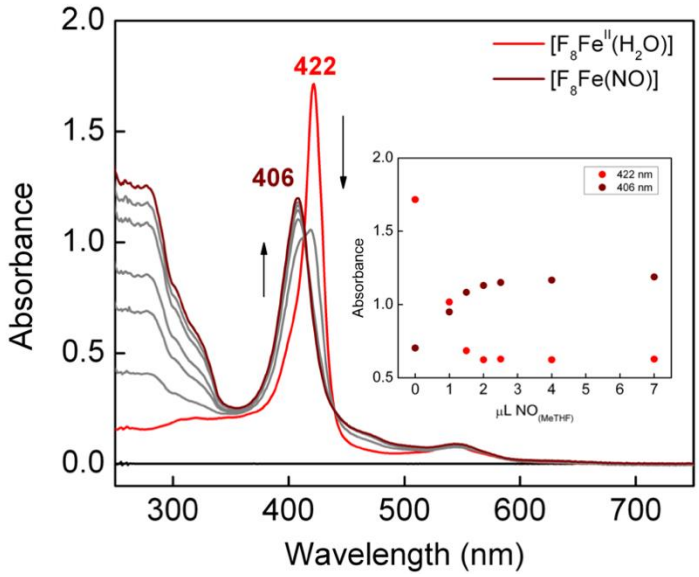

Figure S24 Titration of $NO_{(MeTHF)}$ into 8.2 μM of $[F_8Fe^{II}(H_2O)]$ (Soret = 422 nm) to give the $\{FeNO\}^7$ complex $[F_8Fe^{II}(NO)]$. The concentration of $NO^{\bullet}$ in the MeTHF was determined to be ~21 mM.

24. Titration of $[Cu^{II}(TMG_3tren)(O_2^{\bullet-})]^+$ with $NO_{(MeTHF)}$

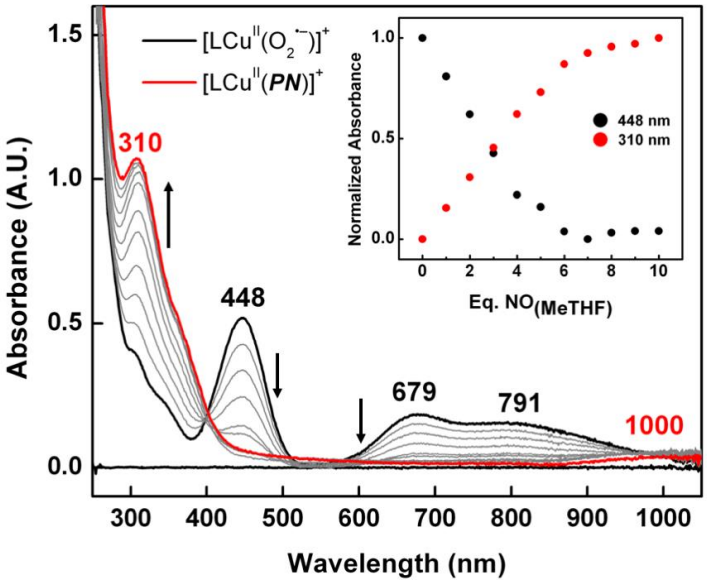

Figure S25 Titration of $[Cu^{II}(TMG_3tren)(O_2^{\bullet-})]^+$ (0.15 mM) with $NO_{(MeTHF)}$ at –125 ºC. Maximal formation occurs at approximately 7 equivalent of $NO_{(MeTHF)}$ added.

25. Conversion of PN1 to PN2 by UV-vis Spectroscopy

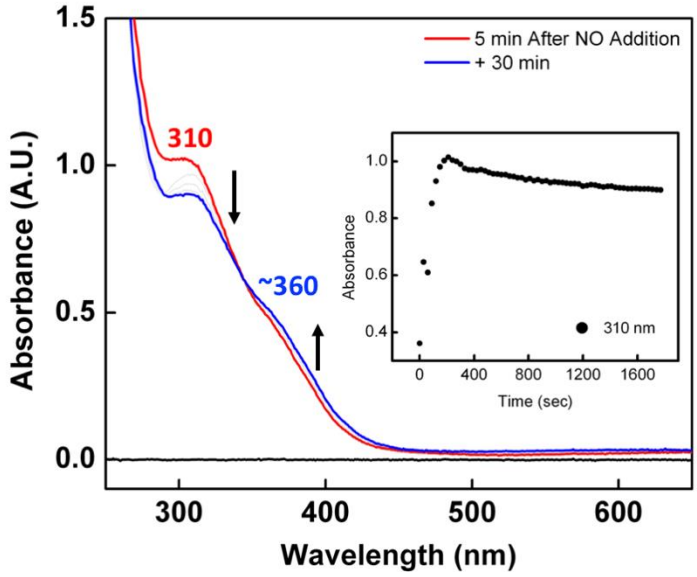

Figure S26 Reaction of $[Cu^{II}(TMG_3tren)(O_2^{\bullet-})]^+$ (0.17 mM) with $NO_{(MeTHF)}$ (0.14 mL, 7 equiv) at –100 ºC in MeTHF. In the first 5 minutes **PN1** forms, and then decays to generate $[Cu^{II}(TMG_3tren)(\kappa^2\text{-}O,O'\text{-}OONO)]^+$ (**PN2**).

26. EPR Fitting of the Conversion from PN1 to PN2

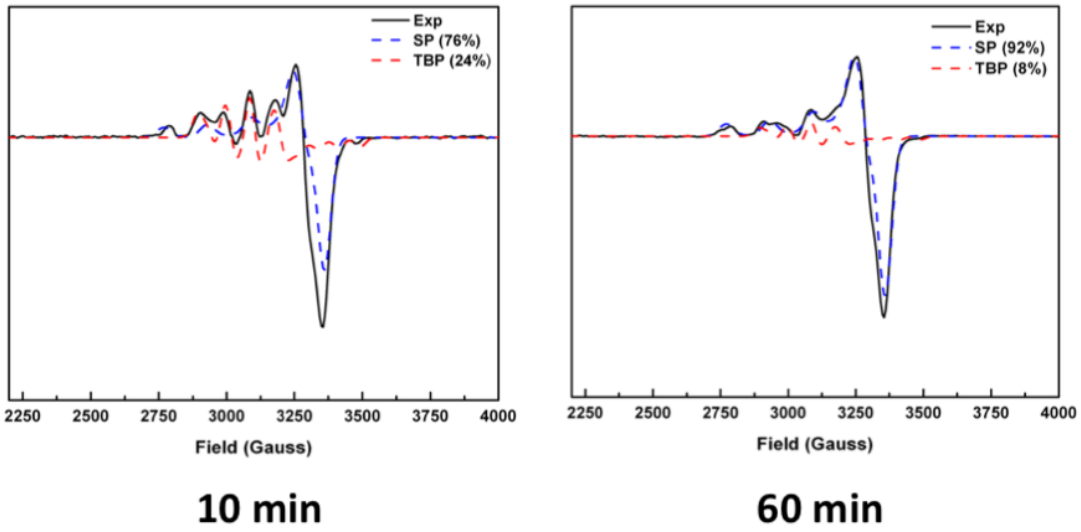

Figure S27 Representative EPR fits of the conversion from **PN1** to **PN2** using EasySpin. EPR parameters used for **PN1** and **PN2** were set constant letting only the relative weights of each component vary.

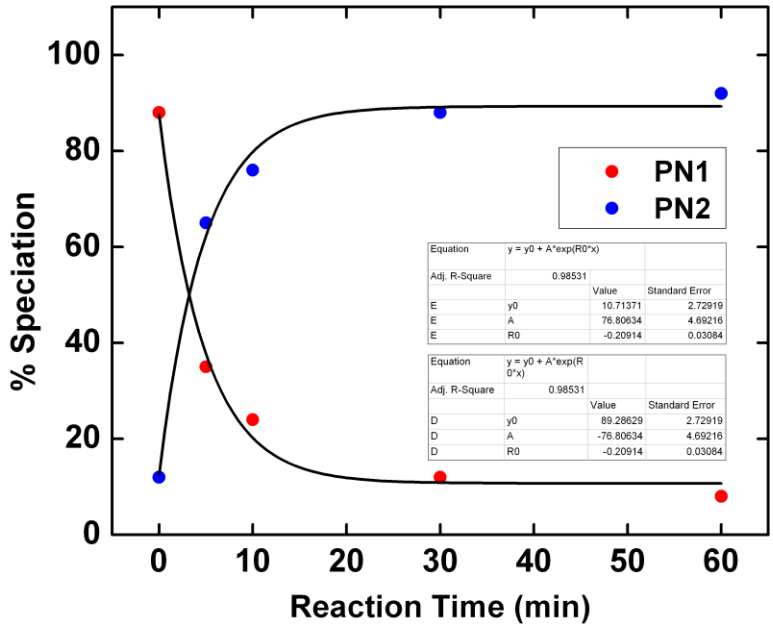

Figure S28 Fitting the of the **PN1** to **PN2** conversion as monitored by EPR to a single exponential. An approximate rate constant was calculated as 3.5 x 10^{-3} s^{-1}.

27. Reaction of $[Cu^{I}(TMG_3tren)]^+$ with $NO_2^{\bullet}$

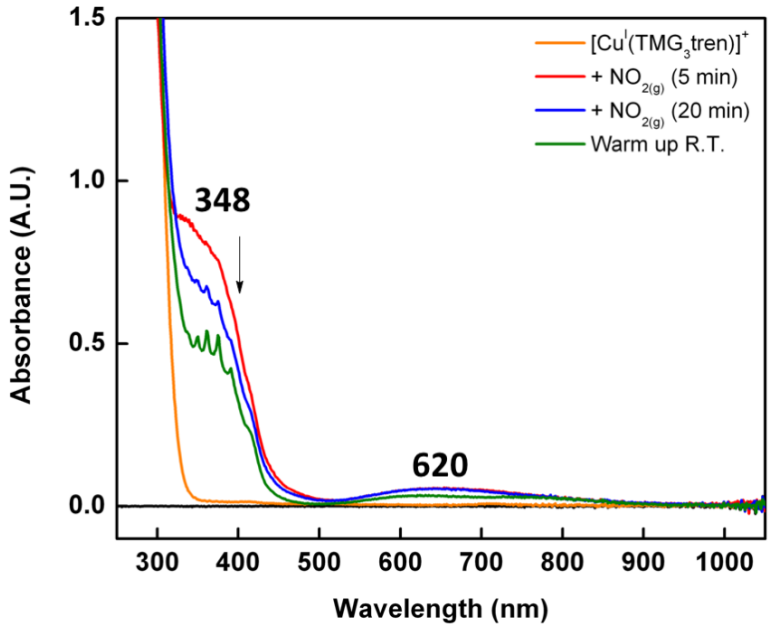

Figure S29 Addition of $NO_2^{\bullet}$ (5 mL) to $[Cu^{I}(TMG_3tren)]^+$ (orange) (0.2 mM) at – 60 ºC in MeTHF. Immediate formation of $[Cu^{II}(TMG_3tren)(\kappa^2\text{-}O,O'\text{-}NO_2)]^+$ occurs (red). Over time the excess $NO_2^{\bullet}$ reacts with solvent to make HNO_2 as evidenced by the sharp features growing centered around 360 nm (blue). Upon warm-up the sharp features become more pronounced (green).

28. Reaction of $[Cu^{I}(TMG_3tren)]^+$ with $NO_{(MeTHF)}$

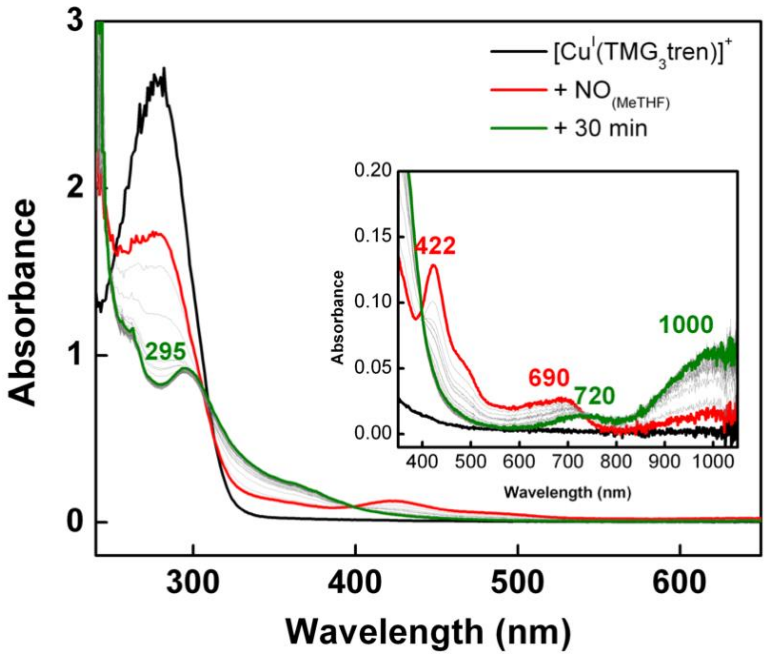

Figure S30 Reaction of $[Cu^{I}(TMG_3tren)]^+$ (**black**, 0.16 mM) with $NO_{(MeTHF)}$ (7 equiv) at –135 ºC in MeTHF. Immediately after $NO_{(MeTHF)}$ addition a transient intermediate (red) forms and rapidly decays to $[Cu^{II}(TMG_3tren)(NO_2^-)]^+$ (green) over the course of 30 mins.

29. NO• Quantification via Addition of [F8Fe(H2O)]

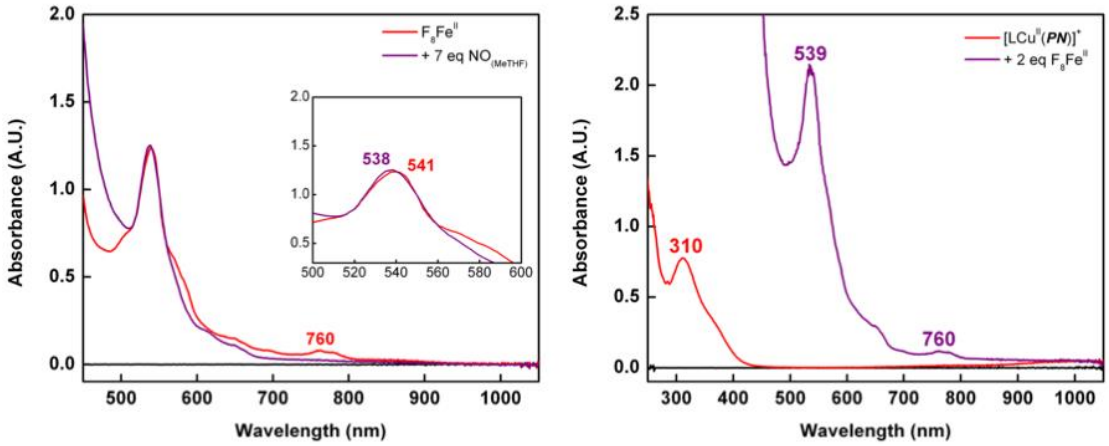

Figure S31 (Left) Reaction of $[F_8Fe(H_2O)]$ (red, 0.11 mM) with $NO_{(MeTHF)}$ (7 equiv) at –125 ºC in MeTHF. (**Right**) Addition of 2 equiv of $[F_8Fe(H_2O)]$ to **PN1** (0.10 mM, red) in MeTHF (purple), –125 ºC following $Ar_{(g)}$ sparging of the solution. Negligible free NO• was detected based on the Fe^{II} feature at 760 nm.

30. Selected Metrical Parameters for the Calculated Structure for *cis*-PN2

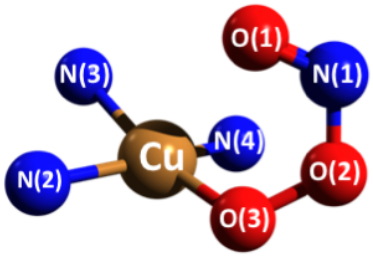

$\tau = 0.05$

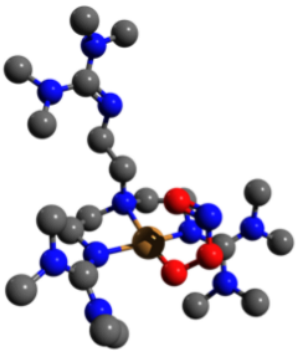

	Distance (Å)		Angle (°)
Cu-N(2)	2.005	N(3)-Cu-O(3)	164.5
Cu-N(3)	2.089	N(2)-Cu-N(4)	161.8
Cu-N(4)	1.993	Cu-O(3)-O(2)	113.2
Cu-O(1)	2.698	N(2)-Cu-N(3)	83.7
Cu-O(3)	1.966		
O(3)-O(2)	1.407	O(3)-O(2)-N(1)-O(1)	–4.5
O(2)-N(1)	1.373	Cu-O(3)-O(2)-N(1)	52.9
N(1)-O(1)	1.190	Cu-O(2)-N(1)-O(1)	26.1

Figure S32 Optimized geometry and selected metrical parameters for *cis*-**PN2** An initial guess geometry derived from the X-ray crystal structure for [Cu^{II}(TMG$_2$dien)(κ^2-*O*,*O'*-NO_2)]SbF_6. Optimization was performed at the b3lyp level of theory using the spin unrestricted formulism, and the D3 dispersion correction. Def2-TZVP was used as the basis set for all atoms. The polarizable continuum model (PCM) using the THF parameters was used to model MeTHF solvation.

Table S2 Experimental X-ray crystallography data for [Cu^{II}(TMG$_2$dien)(κ^2-*O*,*O'*-NO_2^-)]$B(C_6F_5)_4$

Crystal data for [Cu^{II}(TMG$_2$dien)(κ^2-*O*,*O'*-NO_2^-)]$B(C_6F_5)_4$	
Chemical formula	$C_{24}BF_{20}\cdot C_{15}H_{35}CuN_8O_2\cdot C_4H_8O$
M_r	1174.20
Crystal system, space group	Monoclinic, $P2_1/c$
Temperature (K)	110
a, *b*, *c* (Å)	13.4434 (3), 13.0127 (2), 28.0517 (5)
β (°)	100.8508 (19)
V (Å^3)	4819.48 (16)

Z	4
Radiation type	Mo $K\alpha$
μ (mm^{-1})	0.58
Crystal size (mm)	0.37 × 0.23 × 0.05
Data collection	
Diffractometer	SuperNova, Dual, Cu at zero, Atlas
Absorption correction	Gaussian *CrysAlis PRO* 1.171.39.29c (Rigaku Oxford Diffraction, 2017) Numerical absorption correction based on gaussian integration over a multifaceted crystal model Empirical absorption correction using spherical harmonics, implemented in SCALE3 ABSPACK scaling algorithm.
T_{min}, T_{max}	0.318, 1.000
No. of measured, independent and observed [$I > 2\sigma(I)$] reflections	78298, 11069, 9615
R_{int}	0.033
$(\sin \theta/\lambda)_{max}$ ($Å^{-1}$)	0.650
Refinement	
$R[F^2 > 2\sigma(F^2)]$, $wR(F^2)$, S	0.033, 0.084, 1.04
No. of reflections	11069
No. of parameters	787
No. of restraints	385
H-atom treatment	H-atom parameters constrained
$\Delta\rho_{max}$, $\Delta\rho_{min}$ (e $Å^{-3}$)	0.54, -0.47

Computer programs: *CrysAlis PRO* 1.171.39.29c (Rigaku OD, 2017), *SHELXS2018*/3 (Sheldrick, 2018), *SHELXL2018*/3 (Sheldrick, 2018), *SHELXTL* v6.10 (Sheldrick, 2008).[9]

31. DFT Structure Coordinates

$[Cu^{II}(TMG_3tren)(cis\text{-}OONO)]^+$; (charge: +1, multiplicity: 2)

O	0.17028	0.20922	-1.41909	N	-3.69424	-2.19616	0.12642
N	0.03484	0.06758	2.67771	N	1.80030	-2.71314	-0.84050
N	0.19083	2.13530	0.80450	N	3.82296	-1.97778	0.03146
N	-1.85509	-0.88443	0.82135	Cu	0.02931	0.03239	0.52451
N	1.76361	-1.15485	0.85893	C	0.28581	1.46648	3.10228
N	1.43792	2.89181	-0.99041	H	1.36234	1.62815	3.11109
N	-0.12165	4.32321	-0.04181	H	-0.08646	1.62181	4.12027
N	-3.22666	-0.16715	-0.90052	C	-0.33800	2.44817	2.12214

H	-1.42890	2.35545	2.15472	H	-4.76176	-0.17867	-2.35605
H	-0.09683	3.46768	2.43534	H	-3.71907	-1.61561	-2.33592
C	-1.30009	-0.40684	3.11187	C	-2.82861	1.22070	-0.75617
H	-1.98175	0.44199	3.09839	H	-2.71026	1.44672	0.29961
H	-1.25129	-0.78281	4.13926	H	-3.60951	1.85729	-1.17690
C	-1.83317	-1.46521	2.15691	H	-1.88059	1.42508	-1.25771
H	-1.19387	-2.35297	2.19577	C	-5.13596	-2.12884	-0.05717
H	-2.82718	-1.77099	2.49262	H	-5.46115	-1.09285	-0.09523
C	1.11664	-0.83686	3.13779	H	-5.62830	-2.61531	0.78910
H	0.72357	-1.85162	3.16476	H	-5.45597	-2.63397	-0.97344
H	1.42393	-0.56730	4.15346	C	-3.16526	-3.51695	0.41888
C	2.28851	-0.80065	2.16758	H	-2.08227	-3.50691	0.36436
H	2.73624	0.19895	2.17027	H	-3.53780	-4.22692	-0.32434
H	3.05918	-1.49698	2.50963	H	-3.46712	-3.87047	1.40933
C	0.47254	3.08615	-0.04903	C	2.45445	-1.90739	0.04170
C	1.24141	3.27848	-2.38119	C	2.24725	-2.89696	-2.21235
H	1.17562	2.37763	-2.99548	H	1.43841	-2.63004	-2.89500
H	2.06869	3.89907	-2.73502	H	2.53534	-3.93377	-2.40790
H	0.31384	3.83318	-2.49155	H	3.09420	-2.24918	-2.42159
C	2.51648	1.94880	-0.76102	C	0.49235	-3.25470	-0.51609
H	2.68263	1.85254	0.30854	H	0.38847	-3.32134	0.56386
H	3.42424	2.33286	-1.23229	H	0.41318	-4.25705	-0.94310
H	2.28599	0.96477	-1.17192	H	-0.31564	-2.63925	-0.90839
C	0.59639	5.53685	-0.40005	C	4.66132	-0.82465	0.30974
H	1.66105	5.33365	-0.47209	H	4.06636	0.08079	0.30446
H	0.43437	6.29121	0.37436	H	5.42201	-0.73688	-0.47007
H	0.25049	5.94869	-1.35322	H	5.16916	-0.91067	1.27479
C	-1.52547	4.50959	0.27981	C	4.54039	-3.21163	-0.25363
H	-2.03276	3.55287	0.31882	H	3.85458	-4.05411	-0.24764
H	-1.99695	5.11130	-0.50174	H	5.29553	-3.37306	0.51970
H	-1.66263	5.02360	1.23563	H	5.04740	-3.17433	-1.22243
C	-2.88522	-1.09061	0.03782	O	-0.57914	-0.73367	-2.14934
C	-3.73911	-0.53687	-2.21161	N	-0.38792	-0.68840	-3.50529
H	-3.10369	-0.09752	-2.98238	O	0.38193	0.12465	-3.90276

$[Cu^{II}(TMG_3tren)(trans\text{-}OONO)]^+$; (charge: +1, multiplicity: 2)

O	-0.27844	-0.06075	1.45421	C	0.81902	-1.06418	-3.10309
N	-0.30727	-0.22297	-2.63444	H	1.69498	-0.42845	-3.22043
N	-2.13721	-0.81924	-0.61361	H	0.58409	-1.49610	-4.08167
N	0.25298	1.94935	-0.94294	C	1.14293	-2.14239	-2.07957
N	1.45093	-1.47135	-0.82495	H	0.28906	-2.81991	-1.97518
N	-2.41927	-2.10956	1.28400	H	1.98082	-2.73859	-2.45055
N	-4.26620	-1.01938	0.39828	C	-2.92197	-1.28138	0.32493
N	-0.67615	3.19657	0.77253	C	-2.74962	-1.93874	2.69148
N	1.12122	4.07964	-0.39899	H	-1.85447	-1.62394	3.23380
N	3.14087	-1.01932	0.68839	H	-3.11868	-2.87176	3.12460
N	2.89840	-3.19359	-0.09789	H	-3.50684	-1.16938	2.81266
Cu	-0.15879	-0.07874	-0.48964	C	-1.24128	-2.91613	1.02243
C	-1.61413	-0.85050	-2.94921	H	-1.19110	-3.14125	-0.03976
H	-1.48691	-1.93105	-2.91312	H	-1.32615	-3.84996	1.58263
H	-1.92521	-0.58208	-3.96418	H	-0.32667	-2.39906	1.31758
C	-2.66256	-0.45711	-1.92003	C	-5.22906	-1.99909	0.87814
H	-2.86279	0.61706	-1.99288	H	-4.75757	-2.97360	0.96832
H	-3.59968	-0.97254	-2.14757	H	-6.05236	-2.07231	0.16286
C	-0.22005	1.15871	-3.16192	H	-5.64686	-1.71787	1.84966
H	-1.21236	1.60389	-3.10827	C	-4.82463	0.27220	0.03801
H	0.08601	1.14308	-4.21346	H	-4.03307	1.00298	-0.08084
C	0.72841	1.99877	-2.31812	H	-5.48407	0.61384	0.84007
H	1.74631	1.60553	-2.40744	H	-5.40771	0.22493	-0.88628
H	0.74458	3.01710	-2.71487	C	0.24990	3.03664	-0.21113

C	-0.35379	3.80279	2.05554	H	3.52329	-0.66196	2.70794
H	-0.57287	3.09058	2.85347	H	4.84917	-1.46927	1.86459
H	-0.93789	4.71115	2.22519	H	3.37369	-2.36607	2.27674
H	0.70378	4.04446	2.10538	C	3.28041	0.37615	0.31378
C	-1.95680	2.51593	0.71039	H	2.98722	0.49573	-0.72464
H	-2.20038	2.31169	-0.32885	H	4.32459	0.67777	0.43289
H	-2.72233	3.16772	1.13716	H	2.65455	1.02531	0.92594
H	-1.93484	1.56936	1.25301	C	1.98413	-4.31824	-0.18861
C	0.72608	5.47011	-0.23328	H	0.96606	-3.98419	-0.02375
H	-0.35273	5.54301	-0.12734	H	2.23466	-5.04774	0.58581
H	1.02710	6.03618	-1.11872	H	2.04059	-4.81887	-1.15994
H	1.19924	5.92810	0.64050	C	4.31175	-3.53951	-0.07633
C	2.50782	3.86906	-0.77586	H	4.91966	-2.65166	-0.22722
H	2.76188	2.81871	-0.69201	H	4.52096	-4.23885	-0.89001
H	3.15485	4.43168	-0.09774	H	4.60350	-4.01426	0.86509
H	2.71096	4.20305	-1.79765	O	0.63201	0.83303	2.06537
C	2.45579	-1.89419	-0.10005	N	1.07488	0.29670	3.24586
C	3.76010	-1.40534	1.94721	O	1.81518	1.05420	3.79243

$[Cu^{II}(TMG_3tren)(cis\text{-}\kappa^2\text{-}O,O'\text{-}OONO)]^+$; (charge: +1, multiplicity: 2)

Cu	-1.29054	0.20663	-0.39539	C	-5.23963	-1.45211	0.77606
C	1.42956	3.39770	0.95255	H	-4.91474	-2.07138	1.60590
H	1.30015	2.33488	1.13930	H	-6.20479	-1.81123	0.41162
H	1.61251	3.88950	1.91060	H	-5.35907	-0.43055	1.14352
H	2.30422	3.55637	0.31601	C	-4.40732	-0.42768	-1.29394
C	0.11335	5.39833	0.37776	H	-4.19644	0.55926	-0.88390
H	-0.74431	5.71601	-0.20874	H	-5.43862	-0.44931	-1.65137
H	1.01559	5.82340	-0.06783	H	-3.73379	-0.61424	-2.12591
H	0.01563	5.79128	1.39357	C	1.44502	-0.71505	-0.59102
C	-0.77650	3.13537	-0.10157	C	2.81648	-0.98087	-1.22575
C	-2.44631	4.16602	1.38165	H	1.17195	-1.57417	0.01578
H	-1.61293	4.19358	2.07659	H	1.50493	0.12466	0.09816
H	-3.24739	3.57791	1.83334	N	0.21890	3.94583	0.36363
H	-2.80797	5.18285	1.21137	N	-2.04820	3.52659	0.13485
C	-3.15083	3.14727	-0.73039	N	-0.53239	2.02323	-0.77534
H	-2.76819	2.70906	-1.64698	N	0.32791	-0.45608	-1.53852
H	-3.74122	4.03573	-0.96772	N	-1.96203	-1.65370	-0.63969
H	-3.79320	2.42359	-0.22844	N	-3.16986	-3.42331	0.33385
C	0.65612	1.95995	-1.63340	N	-4.23982	-1.45736	-0.28311
H	1.59493	1.96393	-1.07707	O	-2.59844	-0.18014	2.08796
H	0.69000	2.81978	-2.30726	O	-2.46265	0.78582	1.07343
C	0.56919	0.68241	-2.45004	N	-1.43298	-0.67367	2.62085
H	-0.28720	0.73891	-3.12165	O	-0.42685	-0.29366	2.11127
H	1.46752	0.53870	-3.05532	H	2.68568	-1.68589	-2.05394
C	-0.14997	-1.68317	-2.21497	N	3.68765	-1.60253	-0.25379
H	0.67538	-2.25461	-2.64557	H	3.46475	0.99629	0.63383
H	-0.80788	-1.37068	-3.02520	C	4.82767	-1.09032	0.06003
C	-0.94291	-2.52421	-1.22568	N	5.78744	-1.89610	0.64850
H	-1.40006	-3.36836	-1.74728	N	5.23062	0.22334	-0.16067
H	-0.26771	-2.94490	-0.47696	C	4.36085	1.34262	0.12647
C	-3.09166	-2.17012	-0.19259	C	6.57164	0.56783	-0.59412
C	-2.09416	-3.98040	1.14090	C	5.60339	-3.33591	0.60931
H	-1.53323	-4.74818	0.60140	C	6.51617	-1.42782	1.82097
H	-2.52527	-4.43388	2.03553	H	5.23271	-3.63715	-0.36705
H	-1.41555	-3.19248	1.45402	H	4.89181	-3.68441	1.36747
C	-4.32973	-4.28538	0.15079	H	6.56676	-3.81527	0.79328
H	-4.99202	-3.86654	-0.60161	H	7.13051	-0.33483	-0.82597
H	-4.88652	-4.41887	1.08212	H	7.55549	-1.76062	1.78171
H	-3.99157	-5.26670	-0.18936	H	6.06422	-1.82228	2.73965

H	6.50008	-0.34377	1.87681	H	3.22016	-0.06288	-1.66396
H	7.11995	1.13019	0.17113	H	4.06795	1.88940	-0.77726
H	6.52314	1.18919	-1.49460	H	4.86956	2.04967	0.79139

References

[1] M. P. Schopfer, B. Mondal, D. Lee, A. A. N. Sarjeant, K. D. Karlin, *J. Am. Chem. Soc.* **2009**, *131*, 11304–11305.

[2] M. P. Lanci, V. V. Smirnov, C. J. Cramer, E. V. Gauchenova, J. Sundermeyer, J. P. Roth, *J. Am. Chem. Soc.* **2007**, *129*, 14697–709.

[3] R. A. Ghiladi, R. M. Kretzer, I. Guzei, A. L. Rheingold, Y. M. Neuhold, K. R. Hatwell, A. D. Zuberbühler, K. D. Karlin, *Inorg. Chem.* **2001**, *40*, 5754–5767.

[4] J. England, Y. Guo, K. M. Van Heuvelen, M. A. Cranswick, G. T. Rohde, E. L. Bominaar, E. Münck, L. Que, *J. Am. Chem. Soc.* **2011**, *133*, 11880–11883.

[5] A. W. Addison, T. N. Rao, J. Reedijk, J. van Rijn, G. C. Verschoor, *J. Chem. Soc. Dalt. Trans.* **1984**, *251*, 1349–1356.

[6] D. Maiti, D.-H. Lee, A. A. Narducci Sarjeant, M. Y. M. Pau, E. I. Solomon, K. Gaoutchenova, J. Sundermeyer, K. D. Karlin, *J. Am. Chem. Soc.* **2008**, *130*, 6700–6701.

[7] C. X. Zhang, H. C. Liang, E. I. Kim, J. Shearer, M. E. Helton, E. I. Kim, S. Kaderli, C. D. Incarvito, A. D. Zuberbühler, A. L. Rheingold, et al., *J. Am. Chem. Soc.* **2003**, *125*, 634–635.

[8] T. Matsumoto, H. Furutachi, M. Kobino, M. Tomii, S. Nagatomo, T. Tosha, T. Osako, S. Fujinami, S. Itoh, T. Kitagawa, et al., *J. Am. Chem. Soc.* **2006**, *128*, 3874–3875.

[9] G. M. Sheldrick, *Acta Crystallogr. Sect. C Struct. Chem.* **2015**, *71*, 3–8.